Experimental investigation of the noise radiated by a ducted air flow discharge though diaphragms and perforated plates

Paul Laffay, Stéphane Moreau, Marc Jacob, Josselin Regnard

Experimental investigation of the noise radiated by a ducted air flow discharge though diaphragms and perforated plates

P. Laffay [a, *], S. Moreau [b], M.C. Jacob [b, c], J. Regnard [d]

[a] Safran Aircraft Engines, 77500 Moissy-Cramayel, France and Univ Lyon, École Centrale de Lyon, INSA Lyon, Université Claude Bernard Lyon 1, CNRS, LMFA, F-69134, Écully, France
[b] Univ Lyon, École Centrale de Lyon, INSA Lyon, Université Claude Bernard Lyon 1, CNRS, LMFA, F-69134, Écully, France
[c] Institut Supérieur de l'Aéronautique et de l'Espace, ISAE-SUPAERO, F-31400, Toulouse, France
[d] Safran Aircraft Engines, 77500, Moissy-Cramayel, France

Keywords:
Flow discharge
Jet noise
Confined jet
Base pressure oscillations
Perforated plate
Diaphragm

A B S T R A C T

An experimental investigation of the noise radiated by a ducted high pressure flow discharge through diaphragms and perforated plates is carried out for a large range of subsonic and supersonic operating conditions (Nozzle Pressure Ratio (NPR) from 1.2 to 3.6). A parametric study of the geometrical parameters is also conducted to characterize their influence on the acoustic radiation. This covers configurations from single diaphragms to multi-perforated plates with variable hole diameters and arrangements that are placed inside a cylindrical duct. Compared with the free discharge analysed in a first part of the study (perforated plates placed directly at the output of the duct), the discharge into a duct, which is closer to the practical applications, generates strong acoustic modifications. As expected, the broadband noise is disturbed by strong modulations due to acoustic resonances in the output duct (longitudinal resonances and transversal duct modes). However, as in the free configuration, a strong effect of the plate geometries on the mixing noise is observed, allowing to adapt or reduce this source. In particular, the increase of the ratio between the perforation spacing and the perforation diameter allows reducing the maximum amplitude of the mixing noise. Compared to the free-field discharge, the Sound Pressure Level (SPL) in the ducted configuration is on average proportional to the 6-th power of the velocity instead of the 8-th power. Moreover, there are two dominant frequency humps in the sound spectra. The low frequency one is characterized by a constant Helmholtz number, suggesting that the sound is shaped by the duct geometry, whereas the high frequency one is characterized by a constant Strouhal number suggesting that the sound is directly generated by the flow. Finally, for supersonic operating points, the screech radiation appearing with diaphragms in the free configuration is suppressed when the output duct is added but new high amplitude and low frequency tones appear for the largest diaphragms and perforated plates. These lines are due to a coupling between normal shock oscillations and longitudinal resonances.

* Corresponding author.
E-mail address: laffaypaul@gmail.com (P. Laffay).

https://doi.org/10.1016/j.jsv.2020.115177

1. Introduction

In a large number of industrial applications, valves are used to discharge or regulate pressurized fluid flows such as on steam valves in power plants or air valves in aircraft engines. A common way to reduce this pressure is to generate pressure losses by forcing the flow through diaphragms or perforated plates. However forcing high pressure flows though these contractions, generates high speed jets that are responsible for a high level sound emission and might even lead to structural damage.

In an attempt to reduce the acoustic radiation of such devices, an experimental study has been carried out to identify the different acoustic sources generated when a high pressure flow is discharged though perforated plates or diaphragms. A first part of this study has focused on the noise radiated when the flow is released into a free environment, which means that the perforated plate is placed directly at the output of the duct [1]. The aim of this configuration was to analyze the different acoustic sources of the flow leaving the perforations in a free-field configuration in order to assess their intrinsic characteristics. As a reminder, the operating point in this study was defined by the ratio of the total pressure upstream of the perforated plate or diaphragm p_t to the ambient pressure p_a that is the Nozzle Pressure Ratio (NPR). In this first part of the study, various acoustic behaviors have been observed. For diaphragms, far-field acoustic spectra are dominated by mixing noise for all NPRs and by shock-associated noise (screech and BroadBand Shock Associated Noise (BBSAN)) when the critical value of the NPR delimiting the subsonic and supersonic behavior (NPRc = 1.89) is exceeded. For perforated plates, the mixing noise is still present but is composed of two humps. The achieved parametric study has shown that the first hump is associated to the noise of the downstream large equivalent jet resulting from the merger of all individual small jets while the second is associated with the noise of these small jets issuing from the perforations. The noise associated with supersonic phenomena (screech and BBSAN) has also been observed for perforated plates only in the case of perforations in close proximity. In this case, it behaves as a diaphragm. Finally, for low subsonic operating points a high frequency tonal noise component has been observed with the perforated plates as well as with the smallest diaphragm. This sound component has been attributed to the generation of vortex shedding due to the sharp edge combined with acoustic resonances.

The present article is devoted to the second part of the study. The flow discharge is now operated in a duct, which is closer to configurations found in classical industrial applications (Fig. 1). The interaction of the turbulent flow issuing from the discharge though diaphragms or perforated plates with pipe walls/boundary layers and the acoustic propagation in the duct most likely modify the different acoustic sources identified in the free-field case. The objective of the present study is to analyze these modifications induced by the output pipe on the radiation of the discharge system.

One of the first studies on the noise generated by an aerodynamic source in a pipe was proposed by Davies and Ffowcs Williams [2]. They extended Lighthill's analysis [3,4] of the noise radiated by a finite region of turbulence into a quiet medium to that radiated in an infinitely long, straight, hard-walled pipe. In this study, they showed that for turbulent eddies that are small compared with the duct dimensions, the power radiated below the cut-off frequency (when only the plane mode propagates) evolves according to the sixth power of the flow velocity. At high frequencies however, many modes propagate and the duct no longer has a significant influence on the radiation. Similarly to the free-field case, the sound then nearly increases as the eighth power of the velocity.

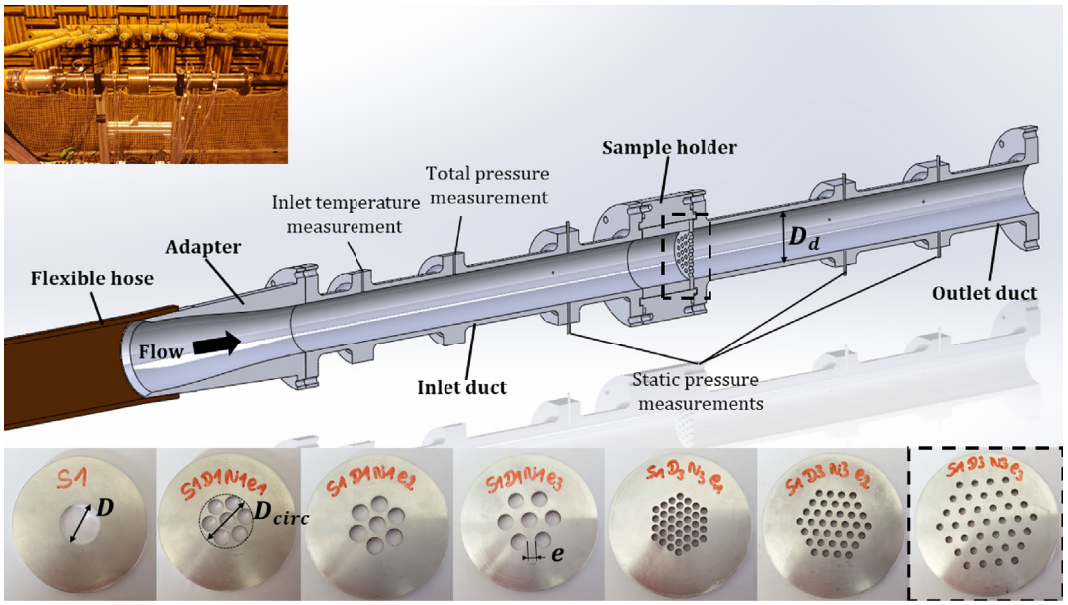

Fig. 1. Experimental setup and a few plate samples tested.

In most cases encountered in duct acoustics, the aeroacoustic source is induced by a change in the pipe geometry such as an elbow, a side branch, a cavity or simply a section modification (sudden expansion, diaphragm …). A number of studies about the flow through a diaphragm has been conducted experimentally, analytically and numerically. Indeed, depending on the operating point determined by the flow velocity or flow pressure at the section modification, different aeroacoustic mechanisms may appear. In the case of a transonic flow through a sudden expansion, Anderson et al. [5,6] then Meier et al. [7,8] showed experimentally that the shock cells downstream of the expansion exhibit various unsteady features. Some of these are responsible for a significant acoustic radiation and may also appear in the present configuration.

The following part of the present study is then divided into seven sections. A brief description of the experimental setup is first given. Then, a comparison between the sound radiated in free-field and ducted configurations is carried out in order to identify the acoustic modifications generated by the duct. The next four sections are devoted to a detailed analysis of the different identified aeroacoustic phenomena. Conclusions are drawn in the final section. Some preliminary results were already published by Laffay et al. [9].

2. Experimental set-up

The experiment has been carried out in the supersonic open-jet wind tunnel at École Centrale Lyon (ECL). The detailed description of the anechoic room and airflow facilities is given in Ref. [1]. Compared with the set-up in the free configuration [1], an output duct with similar diameter $D_d = 49$ mm (cross-section S_d) and length $L = 8.2D_d$ is added downstream of the perforated plates. The overall geometry is then more representative of the configurations encountered in practical applications (Fig. 1) where pressure release valves are mounted in pipe systems.

Similar diaphragms and perforated plates as in the free configuration have been tested. Characteristics of each sample are summarized in Table 1. These samples are identified by the diameter D, the mutual spacing e and the number N of their perforations as well as by their total area S. D_{circ} corresponds to the diameter of the circle circumscribed to all the perforations. Finally, note that all perforations have sharp edges and the thickness of each plate is $0.092D_d$, which means that they are thin and that the flow does not re-attach on the wall after separating at the inlet.

In order to analyze the acoustic effects of the output duct, measurements have been carried out for the same operating points as in the free configuration (NPR = 1.2 to 3.6 by steps of 0.2) and similar acoustic devices and acquisition characteristics have also been used. These are specified in Ref. [1]. As a reminder, the NPR is the ratio between the total pressure upstream of the plate and the ambient pressure. The observation angle Θ is defined with respect to the duct axis starting from the downstream direction as shown in Fig. 2. It should be stressed that in the present case, the array is centred on the exit outlet duct, whereas it was centred on the perforated plate in the free jet configuration of [1].

3. Far-field radiation with and without duct

The far-field acoustic radiation measurements obtained in the ducted configurations are first compared to the corresponding free-field results for various NPRs and plates in order to identify the acoustic modifications generated by the output duct. The acoustic post-processing used for the ducted configuration is unchanged compared to the free one and is detailed in Ref. [1].

Table 1
Geometric description of the tested diaphragms and perforated plates.

Name	N	D/D_d $\times 10^{-1}$	e/D_d $\times 10^{-1}$	S/S_d $\times 10^{-1}$	D_{circ}/D_d $\times 10^{-1}$
S1	1	4.31	–	1.86	–
S1D1N1e1	7	1.63	0.20	1.86	5.29
S1D1N1e2	7	1.63	0.41	1.86	5.70
S1D1N1e3	7	1.63	0.82	1.86	6.52
S1D2N2e1	19	0.99	0.20	1.86	5.75
S1D2N2e2	19	0.99	0.41	1.86	6.57
S1D2N2e3	19	0.99	0.82	1.86	8.20
S1D3N3e1	37	0.71	0.20	1.86	6.18
S1D3N3e2	37	0.71	0.41	1.86	7.41
S1D3N3e3	37	0.71	0.82	1.86	9.86
S2	1	2.61	–	0.68	–
S2D2N1e1	7	0.99	0.20	0.68	3.37
S3	1	6.01	–	3.61	–
S3D2N3e1	37	0.99	0.20	3.61	8.14
S4D4N4e4	351	0.31	0.06	3.29	1.00

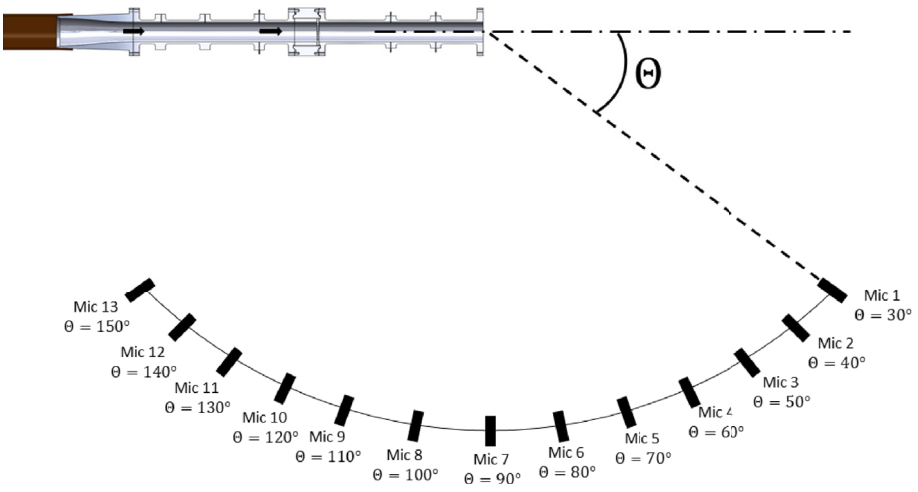

Fig. 2. Position of the microphone array in the ECL large anechoic wind tunnel.

3.1. Far-field acoustic results without output duct

As discussed in the first part of the study [1], the main aeroacoustic characteristics of the diaphragms and the perforated plates have been identified in the free configuration. Fig. 3 summarizes the NPR ranges at which the main aeroacoustic sources are observed. The shades of grey indicate the source mechanisms: mixing noise (light grey), shock associated noise (medium dark grey) and low NPR tonal noise (dark grey). The configurations are specified on the top line. The corresponding obstructions are shown on the bottom line. The NPRs are specified in the left column.

As discussed in the introduction, three main different acoustic phenomena have then been identified: mixing noise, shock-associated noise and low NPR tonal noise. The mixing noise, first of all, is a broadband radiation; it results from the mixing of the flow in the jet shear layers generated by the perforations and therefore appears for all operating points and configurations. In the case of diaphragms, similar characteristics as for the mixing noise of jets issuing from conventional nozzles have been observed [1]. The shapes of the far-field acoustic spectra are found to agree with Tam et al.'s similarity spectra [10] (Fig. 12 in Ref. [1]) and the dual source of the mixing noise has also been identified and discussed in Ref. [1]. In the case of the perforated plates, the mixing noise is strongly modified with two distinct humps in the acoustic spectra. The high frequency hump is due to the radiation of the small isolated jets issuing from the perforations while the low frequency one is attributed to the radiation of the merged jets that form an equivalent jet of larger diameter. These results are consistent with studies on multiple nozzles [11–14]. The modification of the different geometrical parameters of the perforated plates thus allows to tune the mixing noise spectrum. For supersonic regimes, shock-associated noise appears for diaphragms and perforated plates with perforations in close proximity. The associated noise sources, which are both tonal (screech) and broadband (BBSAN), are related to the interaction of instabilities in the shear layer with the shock cells present in the jet. The screech prediction models developed for supersonic jets issuing from conventional convergent nozzles that are not fully expanded show a good agreement with the results obtained in the diaphragm cases. Finally, a tonal noise component has also been

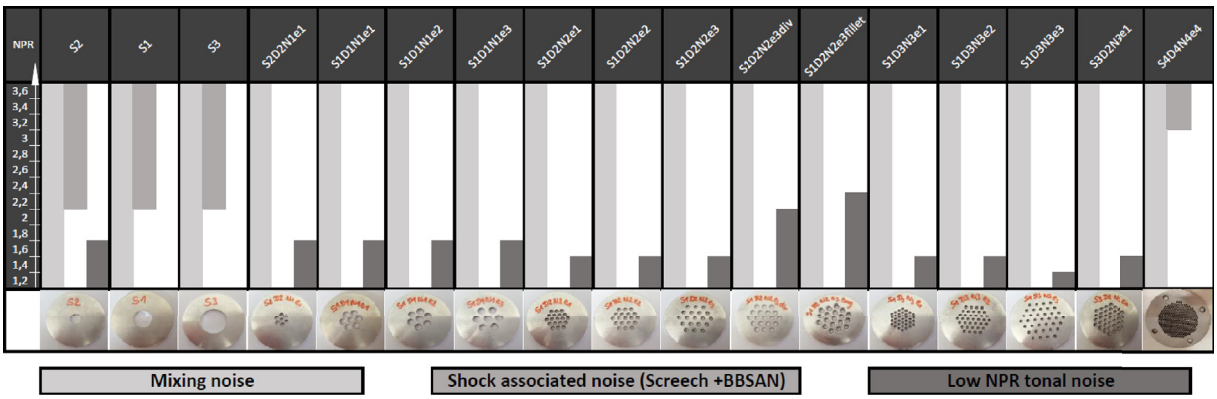

Fig. 3. Summary of the different acoustic phenomena observed without the outlet duct from Ref. [1].

observed at low NPRs for the majority of the perforated plates as well as for the smallest diaphragm. This tone is possibly associated with a feedback loop between instabilities in the flow due to sharp edges and the acoustic field.

3.2. Far-field acoustic results with output duct

In order to investigate the effects of the output duct, the far-field acoustic spectra with and without output duct are now compared in Figs. 4 and 6 for the same configurations, various NPRs and for microphones at $\Theta = 30°$ and $90°$ respectively.

By comparing the far-field acoustic spectra with and without output duct, strong modifications can be identified. Before addressing this issue, note that in both cases the background noise obtained and given by NPR = 1 (null pressure differential between both sides of the plate generating no flow) is far below the noise measured in all configurations. First of all, for the two diaphragms S1 and S3, the shock-associated noise at $\Theta = 30°$ (screech characterized by the high frequency tones in Fig. 4 (a) and (c)) completely disappears with the addition of the duct (Fig. 4 (b) and (d)). This suggests that the duct disrupts the establishment of the feedback loop responsible for the screech. The broadband noise spectra are also altered by more or less pronounced modulations at low and medium frequencies (highlighted by arrows in Fig. 4 (h)). The latter are probably caused by duct resonances. Moreover, the broadband noise level also seems to be modified: the low operating point levels are increased while the high ones are reduced. These modulations of the broadband noise will be studied in Sec. 4 and the level variation in Sec. 6. For the diaphragm S3, in addition to these modifications, strong low frequency tones appear from NPR = 2.2 to 3.4 (Fig. 4 (d)). These tones appear in a particular supersonic NPR range and their frequencies do not match those of the duct resonances as the modulations in the other configurations do. This suggests that they are rather due to an aerodynamic mechanism, which is likely to be non-linear. Therefore in an attempt to validate this assumption, the bicoherence ($b(f_1, f_2)$) is plotted in Fig. 5 for configurations S1 and S3 at NPR 2.4. This signal processing tool allows finding the non-linear interaction in a signal. It is given by the equation:

$$b(f_1,f_2) = \frac{|\sum_n F_n(f_1)F_n(f_2)F_n^*(f_1+f_2)|}{\sqrt{\sum_n |F_n(f_1)|^2 |F_n(f_2)|^2 |F_n^*(f_1+f_2)|^2}}, \tag{1}$$

where F denotes the Fourier transform and * the complex conjugate whereas n refers to the sample index of the averaging procedure. Like the coherence, the bicoherence is bounded between 0 and 1. A bicoherence equal to 1 for two frequencies f_1 and f_2 means that the frequency $f_3 = f_1 + f_2$ is generated by a non-linear interaction between the first two frequencies. In other words, this third frequency is not created by an independent source.

Pronounced differences can be observed between results for the diaphragms S1 and S3 confirming the assumption that the underlying mechanisms are different. For S1, the bicoherence is negligible for all frequencies. There is thus no non-linear interaction, which is consistent with the assumption that modulations in the spectra are due to the acoustic duct resonances as discussed in Sec. 4. For the diaphragm S3 however, the bicoherence equals 1 for each frequency of the high level lines shown in Fig. 4 (d). There are strong non-linear interactions between the different tones. This suggests that these lines are governed by a new single noise source. Moreover, it can be observed that these strong and thin lines at $f = 432$, 648, 864, 1080 Hz (NPR = 2.4) are the exact harmonics of the fundamental frequency $f_0 = 216$ Hz (lowest frequency tone). This source will be studied in Sec. 7. In fact, for the diaphragm S3, the modulations of the broadband spectrum due to longitudinal resonances are less pronounced than for smaller diaphragms (*e.g.* S1) and mainly arise at low NPRs. This may be explained by an increase of the flow rate in the output duct involving an increase of the convection losses at the open pipe termination and inducing a widening of the acoustic resonances peaks in the broadband spectrum.

For perforated plates now, still at $\Theta = 30°$ (Fig. 4 (e)–(h)), similar phenomena as for diaphragms can be observed on the broadband noise: modulations appear on all spectra when the outlet duct is added and their amplitudes relative to the background spectra are modified (increase at low NPRs and decrease at high ones). These modulations also seem to be affected by the plate geometry. Indeed, their amplitudes are increased when the perforation size decreases for a constant cross-section (Sec. 4). Finally, even if the phenomenon is less pronounced, the two humps characteristic of the perforated plate mixing noise shown in Laffay et al. [1] are still present when the output duct is added. Indeed, for perforated plates with widely spaced perforations (Fig. 4 (g) and (h)), a significant increase of the high frequency range appears that is probably due to a later merging of the small jets issuing from the perforations. In fact, the only acoustic behavior that doesn't seem to be strongly modified by the output duct is the tonal noise at low NPRs as shown in Fig. 4 (e) and (f). This noise mechanism will not be analysed in the present study.

For $\Theta = 90°$ (Fig. 6), similar trends can be observed. For diaphragm S1 (Fig. 6 (a) and (b)), the screech (high frequency tones at supersonic operating points) is associated with the BBSAN (high frequency hump) that characterises the sideline radiation of imperfectly expanded jets [15–17]. This radiation also seems to be strongly altered by the addition of the outlet duct. Only a slight hump seems to subsist. Moreover, the broadband spectra without duct are wider than in the downstream direction (Fig. 4 (a)), which is characteristic of the jet mixing noise and the radiation of the small scale turbulence in this direction [18,19]. Again this phenomenon is less pronounced when the outlet duct is added despite a slight decrease of the maximum amplitude compared with the downstream direction. This decrease of the maximum amplitude between $\Theta = 30°$ and $90°$ may be induced by the directivity of the acoustic radiation at the duct output or by the output large jet. Similar conclusions hold for the mixing noise generated by the perforated plate S1D3N3e3 in Fig. 6 (c) and (d).

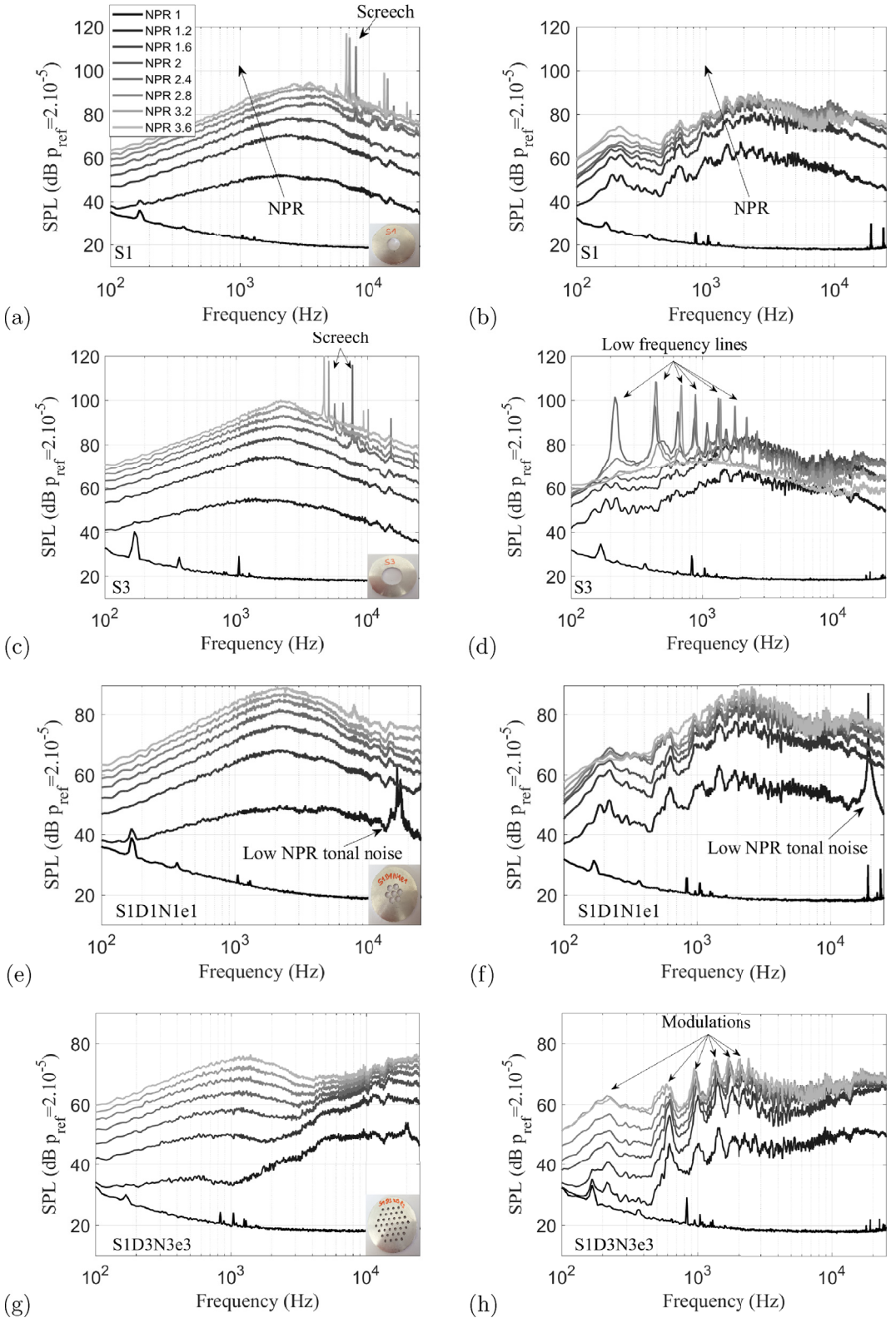

Fig. 4. Comparison of the far-field acoustic spectra for the configurations without (left) and with (right) output duct at $\Theta = 30^{\circ}$ for perforated plates and diaphragms: (a),(b) S1, (c),(d) S3, (e),(f) S1D1N1e1 and (g),(h) S1D3N3e3.

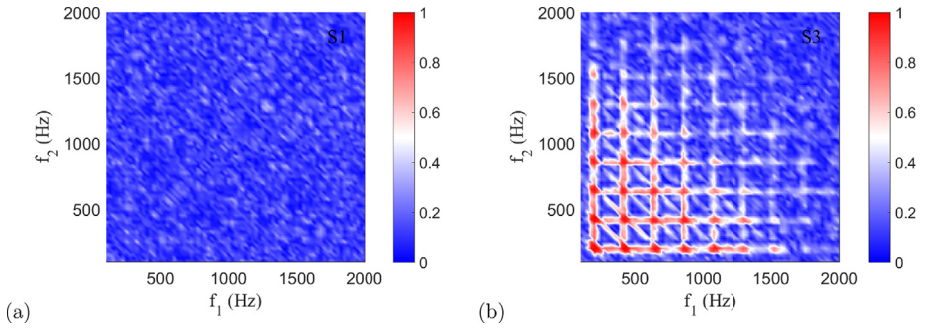

Fig. 5. Bicoherence at NPR = 2.4, Θ = 90° for: (a) S1 and (b) S3.

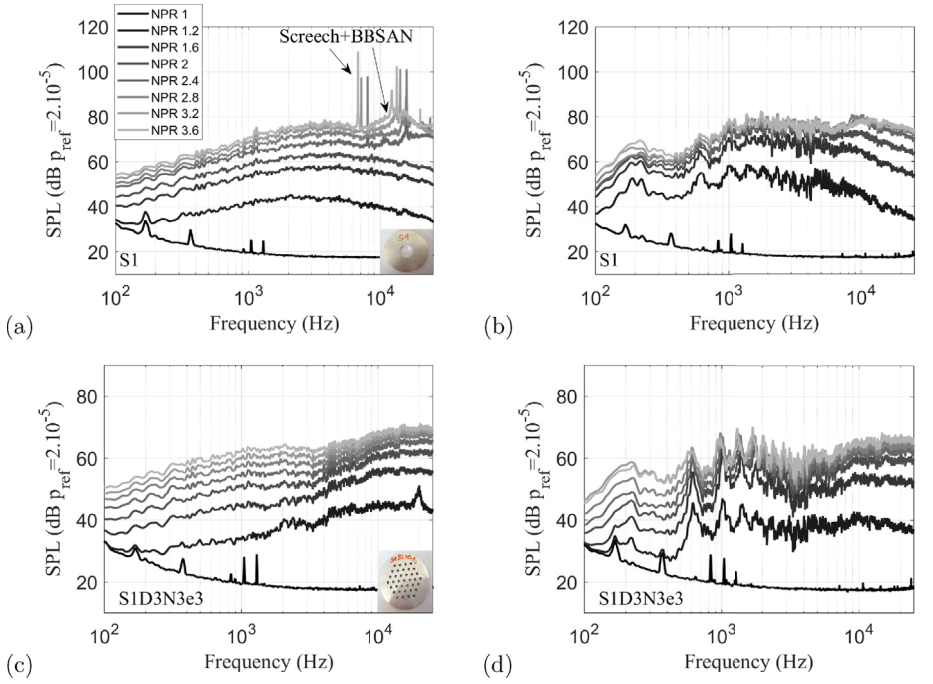

Fig. 6. Comparison of the far-field acoustic spectra for the configurations without (left) and with (right) output duct at Θ = 90° for perforated plates and diaphragms: (a),(b) S1, (c),(d) S1D3N3e3.

The previous comparisons have been performed for two angular positions. Fig. 7 now compares the overall directivity of the radiated noise (OASPL) obtained for perforated plates and a diaphragm with similar total perforation area in the free and ducted configurations at NPR = 2. Note however that the vena contracta effect at the perforation inlet may induce slightly different discharge flow between configurations with equivalent cross-section for equal NPR. The OASPL is obtained by the following relation:

$$OASPL = 10\log\left(\frac{\sum_{f_{min}}^{f_{max}} S_{pp}(f)\Delta f}{p_{ref}^2}\right)[\mathrm{dB}], \tag{2}$$

where S_{pp} is the power spectral density of the acoustic signals and $p_{ref} = 2 \times 10^{-5}$ Pa the reference acoustic pressure. $f_{\min} = 100$ Hz, $f_{\max} = 40000$ Hz and $\Delta f = 8$ Hz is the frequency resolution. For this intermediate NPR, the noise radiated in the ducted configuration is globally louder than in the free one, in particular in the downstream direction. However, the level difference between the two configurations varies as a function of the operating point as shown in Figs. 4 and 6. The trend is reversed for high supersonic NPRs. Moreover, the plate geometry seems to have a stronger effect on the radiated noise compared to the free configuration. The reduction of the perforation diameter associated with the increase of the perforation number in order to conserve a constant cross-section significantly reduces the sound level between 100 and 40000 Hz in all

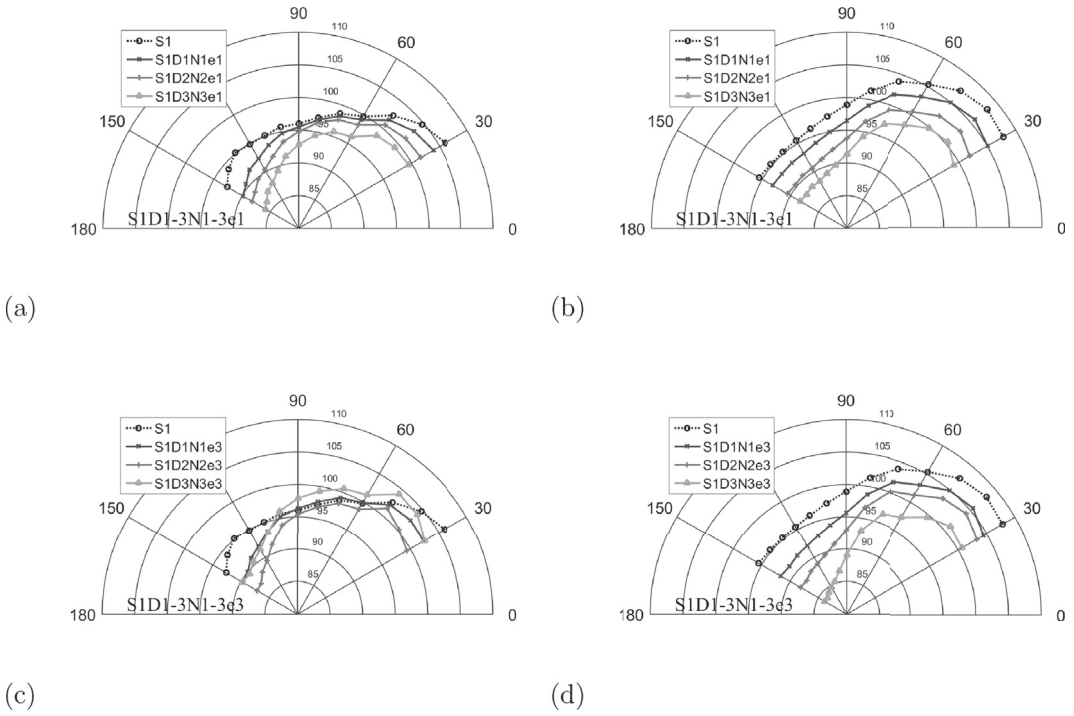

Fig. 7. Comparison of the OASPL directivity as a function of Θ at NPR = 2 for perforated plates with different perforation diameter and number but constant perforation spacing and cross-section; (a),(c) are the free-field configurations and (b),(d) the ducted ones.

studied directions. In the downstream direction ($\Theta = 30°$) for example, the sound radiated by the diaphragm S1 is almost 10 dB louder than for the perforated plate S1D3N3e1 (Fig. 7 (b)).

To summarize, the different acoustic behaviors as well as the operating points at which each regime appears are presented in Fig. 8, to be compared with the free-field case shown in Fig. 3 with the same conventions. The main modification generated by the addition of the output duct is the modulation of the broadband noise. Its origin is examined in the following section.

4. Study of propagation effects

4.1. Identification of the propagation effects

As seen in Fig. 4, adding an output duct generates strong modulations of the broadband component that can emerge up to 15 dB from the spectra typically for diaphragms and perforated plates with small cross-sections (Fig. 9 (a)). Such modulations have been extensively studied in the context of sound propagation in ducts [20,21]. Indeed, in such cases, resonance

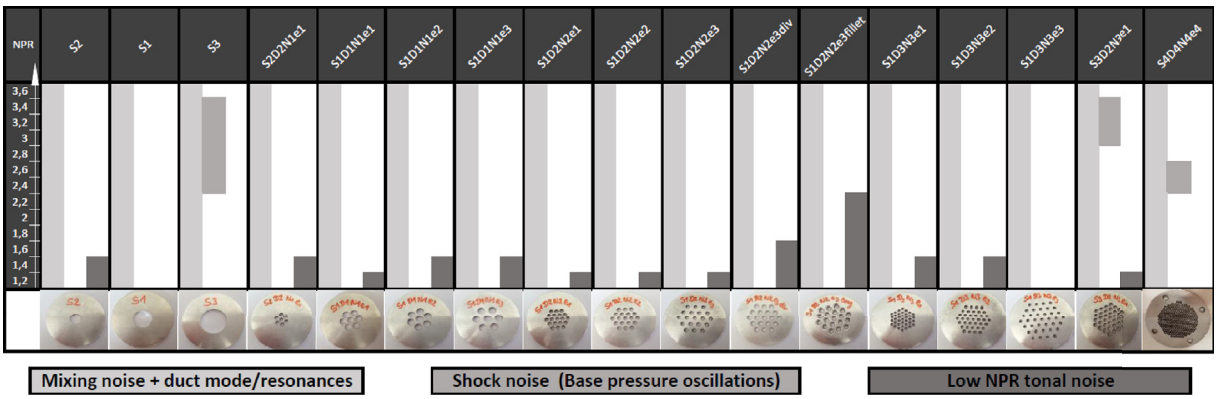

Fig. 8. Summary of the different acoustic phenomena observed with the outlet duct.

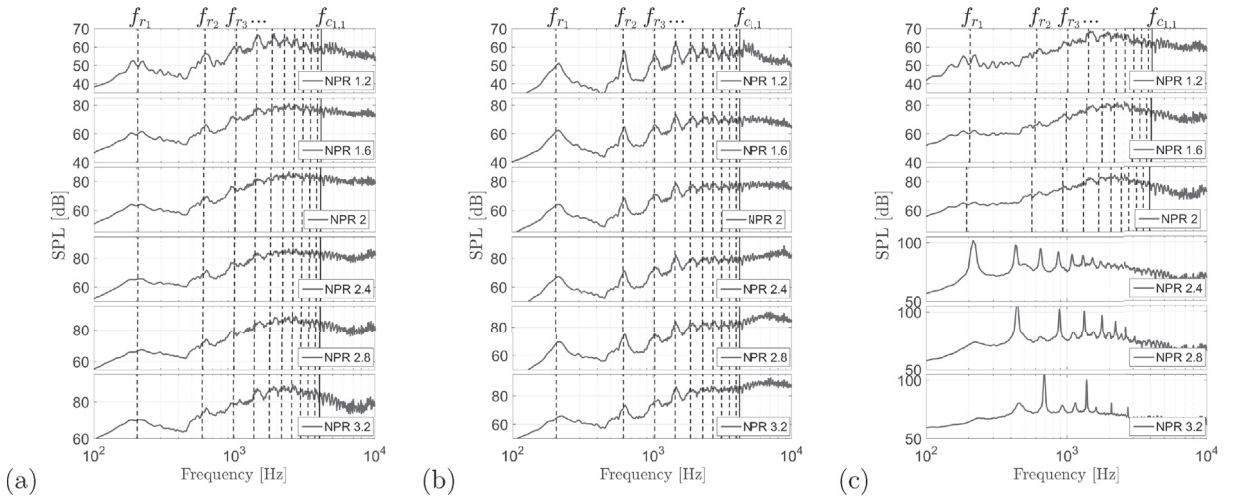

Fig. 9. Far-field acoustic spectra for $\theta = 30°$ and NPR from 1.2 to 3.2 by step of 0.2 for diaphragms: (a) S1, (b) S2 and (c) S3. The dashed black lines are the predicted longitudinal resonance frequencies given by Eq. (6) and the solid black line is the cut-on frequency of the first azimuthal mode given by Eq. (5).

phenomena may occur that are responsible for the sound pressure increase observed here at discrete frequencies. In the case of an infinite cylindrical duct with hard walls and a mean axial flow (Mach number M_x), the acoustic pressure in the duct p can be expressed far from the source region as the sum of modes denoted by μ and m in the radial and azimutal directions respectively. According to Michalke [22,23], or Rienstra & Hirschberg [20], in a cylindrical coordinate system (x, r, ϕ), the general expression of the pressure is then:

$$p(x,r,\phi) = \sum_{m=-\infty}^{+\infty} \sum_{\mu=1}^{+\infty} \left(A_{m\mu} e^{-ik^{+}_{m\mu}x} + B_{m\mu} e^{-ik^{-}_{m\mu}x} \right) U_{m\mu}(r) e^{-im\phi}. \tag{3}$$

$A_{m\mu}$ and $B_{m\mu}$ are the complex modal amplitudes of the left-running wave (wave number $k^{+}_{m\mu}$) and the right-running wave (wave number $k^{-}_{m\mu}$) respectively. They depend on the boundary conditions and the noise source, which is here the turbulence zone caused by the jets exiting the perforations of the plate. $U_{m\mu}(r) = N_{m\mu} J_m(\chi_{m\mu} r)$ is the normalized mode expressed with J_m the m-th order Bessel function of the first kind and $\chi_{m\mu}$ the μ-th zero of its derivative J_m'. $N_{m\mu}$ is a normalization constant. The above wave numbers are defined as:

$$k^{\pm}_{m\mu} = \frac{-kM_x \pm \sqrt{k^2 - \beta^2 \chi^2_{m\mu}}}{\beta^2}, \qquad \beta = \sqrt{1 - M_x^2} \tag{4}$$

where k is the acoustic wave number. According to Eq. (4), a mode (m, μ) will propagate if its frequency exceeds the mode cut-on frequency $f_{c_{m\mu}}$ given by:

$$f_{c_{m\mu}} = \frac{\chi_{m\mu} c_0 \beta}{2\pi}. \tag{5}$$

where c_0 is the speed of sound in the duct. Below this frequency, the modes are cut-off and their amplitude decays exponentially. Before the apparition of the first azimuthal mode $(1, 1)$ for which $\chi_{1,1} = 1.84/R$, only the plane mode propagates and strong longitudinal resonances may appear in the duct due to boundary conditions on the perforated plates and at the open duct end. Given the large Reynolds numbers of the jets issuing from the perforations, the plate is first assumed to behave as a hard wall on which the velocity vanishes, while the open end is approximately equivalent to a pressure node. The resulting quarter-wave frequencies f_{r_n} are then given by:

$$f_{r_n} = (2n-1)\beta^2 \frac{c_0}{4(L+\delta)}, \tag{6}$$

where n is a positive integer and δ is the duct length correction that takes the finite cross-section of the duct into account as well as the end geometry of the flow [20,24–27]. In particular, Peters et al. [27] showed that the end correction for a flanged pipe similar to the present application is $\delta \simeq 0.2R$ for low Strouhal numbers $St = \frac{kR}{M_x} < 0.4$, while $\delta \simeq 0.8R$ for $St > 1$.

In order to predict the resonance frequencies of the longitudinal standing waves for the present geometry, M_x must be determined. However, this requires a large number of assumptions and simplifications since the flow is strongly non-uniform in the duct due to the mixing of multiple jets with various diameters and distributions. The flow at the exit of the perforated plates is first assumed to be isentropic. The mean jet Mach number M_j then becomes

$$M_j = \sqrt{\frac{2}{\gamma - 1}\left[NPR^{\frac{\gamma-1}{\gamma}} - 1\right]}, \tag{7}$$

For a uniform mean flow velocity through the duct cross-section far downstream of the plate and a constant density, mass conservation yields

$$M_x = \Gamma_0 \frac{S}{S_d} M_j, \tag{8}$$

where Γ_0 is the vena contracta factor which can be determined for a sharp edge circular orifice with $S/S_d < 0.6$ and $M_j < 1$, by Refs. [28,29]:

$$\Gamma_0 \simeq \frac{1}{1 + \sqrt{1 - S/S_d}} + \frac{\left(1 + \frac{\gamma-1}{2} M_j^2\right)^{\gamma/(\gamma-1)} - 1}{\gamma M_j^2} - \frac{1}{2}. \tag{9}$$

For $M_j > 1$, the vena contracta factor is approximated by $\Gamma_0 = 0.8$, in agreement with Kayser and Shambaugh's experiments [30]. The resulting values of M_x are summarized in Table 2 as a function of the NPR for the three cross-sections S1, S2 and S3.

The cut-on frequency of the first azimutal mode calculated from Eq. (5) and the longitudinal resonance frequencies given by Eq. (6) are represented in the spectra of Fig. 9 respectively by the solid and dashed lines. The end correction is based on the results of Peters et al. [27] for an flanged duct (between $0.2R$ and $0.8R$ depending on St) and the speed of sound in the duct c_0 is determined as:

$$c_0 = \sqrt{\gamma r T_s}, \tag{10}$$

where $r = 287.06$ J.kg^{-1} K^{-1} and T_s is the static temperature in the duct. Considering M_x given in Table 2 and the total temperature T_t measured at the end of the output duct ($T_t = 302 \pm 3$ K), this temperature can be approximated by:

$$\frac{T_t}{T_s} = 1 + \frac{\gamma - 1}{2} M_x^2. \tag{11}$$

First of all, a very good agreement can be observed between the predicted longitudinal resonance frequencies and modulations appearing in the experimental spectra for the three diaphragms S1, S2 and S3. As discussed previously, the increase of the mass-flow rate and thus of the mean velocity in the output duct by increasing the NPR or the diaphragm section reduces the modulation intensities. This decrease of the resonance amplitude when M_x is increased has also been observed by Ingard and Singhal [24] and has been attributed to interactions between the acoustic field and the turbulent flow in the duct and at its exit. The strong modulations observed in the spectra are thus caused by acoustic longitudinal resonances in the output duct when only the plane mode is propagating ($f < f_{c_{1,1}}$). Finally at the cut-on frequency of the first azimuthal mode ($f_{c_{1,1}}$), a slight jump may be observed in the spectra mainly for low NPR and the smallest diaphragm S2. Since the jump is visible at low NPR, this observation has however to be confirmed.

Table 2
Approximated mean Mach number M_x as a function of the NPR.

	NPR	1.2	1.4	1.6	1.8	2	2.2	2.4	2.6	2.8	3	3.2	3.4	3.6
S1	$M_x(\times 10^{-1})$	0.54	0.78	0.98	1.16	1.56	1.67	1.77	1.86	1.95	2.02	2.09	2.15	2.21
S2		0.19	0.28	0.35	0.41	0.57	0.61	0.65	0.68	0.71	0.74	0.76	0.79	0.81
S3		1.10	1.60	2.00	2.35	3.02	3.25	3.44	3.62	3.78	3.92	4.06	4.18	4.29

4.2. Effect of the perforated plate geometry on the acoustic resonances

The effect of the perforated plate geometry on the resonance amplitude is now studied. For this analysis, perforated plates with constant overall cross-sections have been considered in order to conserve comparable mass-flow rates through the plates. The resonance frequencies have been previously calculated assuming the perforated plate to reflect sound waves as a hard wall. However, sound waves impinging on the perforated plate are likely to be partly transmitted to the upstream side. The perforated plate would then have a finite impedance that would reduce the resonance amplitude compared to the hard wall. Indeed, it can be easily understood that a less reflective plate will generate weaker resonances. Several studies have been conducted to try to determine the impedance of perforated plates as a function of the geometry [31–33]. In particular, they show that the perforation diameter may have an effect on the plate impedance for a given overall cross-section.

In order to analyze the effect of the plate geometry on the resonance amplitude in the present application, Fig. 10 shows the far-field acoustic spectra for various perforated plates with constant cross-section but different perforation numbers N, diameters D and spacings e for $\Theta = 90°$ and NPR = 1.4. From left to right, the perforation spacing increases while from top to bottom, the perforation diameter decreases and the perforation number increases in order to keep the cross-section constant. When e increases for a constant D and N, the resonance amplitude seems to increase for all configurations. In fact the maximum amplitude of the resonance is approximately conserved while the broadband noise decreases leading to a relative increase of this resonance amplitude. The quality factor of the resonant system thus seems to be conserved. Similarly, when N increases and D decreases for a constant e, a relative increase of the resonance amplitude can also be observed.

Note that the perforated plate geometry also modifies the flow field and especially the size of the equivalent jet formed by the merging of the jetlets. The slow flow regions are thus more or less extended and might have an impact on the resonances [28,29]. Further aerodynamic investigations are thus necessary to associate the modification of the resonance amplitude with the variation of the plate impedance or with flow effects.

Now that the effects of the acoustic propagation in the duct have been identified, they can be modelled as in Refs. [9,22,23]. However these models do not precisely predict all the acoustic modifications observed for each configuration and operating point since these are resulting from various mechanisms. Therefore it would be interesting to separate the propagation effects induced by the geometry from the noise sources generated by the flow in order to analyze other noise mechanisms such as the mixing noise. The following section is devoted to such a decomposition.

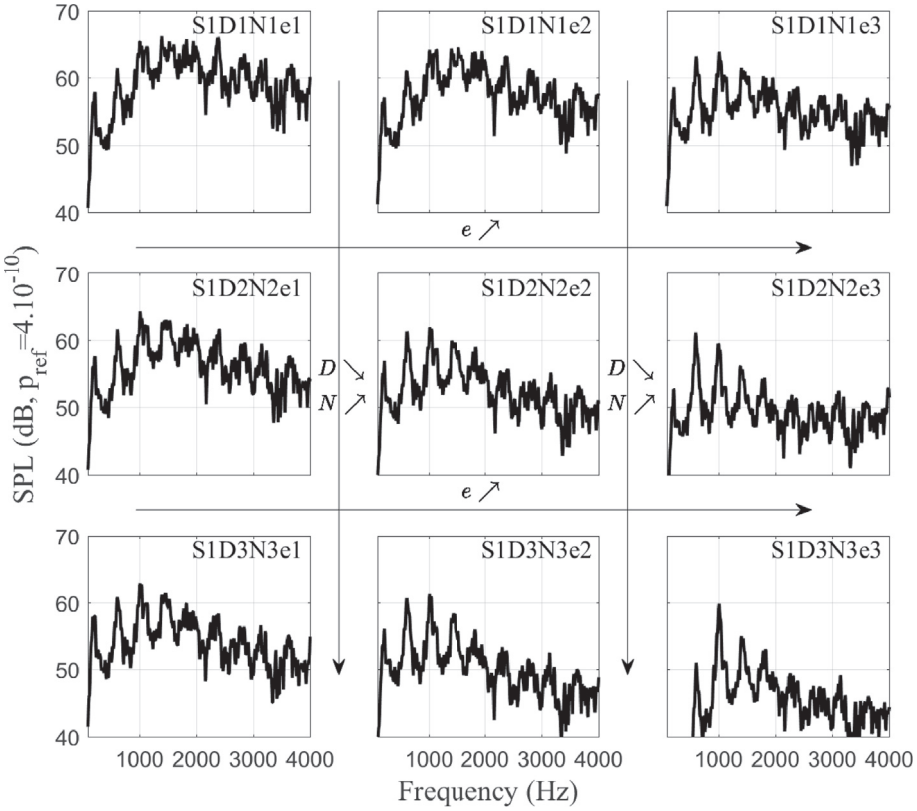

Fig. 10. Far field acoustic spectra for perforated plates with constant cross-section at $\Theta = 90°$ and NPR = 1.4.

5. Decomposition of the source and propagation effects

As mentioned previously, in order to study the broadband noise generated by the mixing of the flow downstream of the perforated plates and diaphragms, it would be interesting to separate it from the sound propagation in the duct identified in Sec. 4 (modulations and jumps) from the measured acoustic spectra. Indeed as shown in Fig. 4, the interaction of the different jets with the duct walls, low speed regions as well as the acoustic field in the duct seems to modify the mixing noise significantly. It is thus not possible to analyze the acoustic propagation effects on the one hand, and the mixing noise based on free-field observations studied in Ref. [1] on the other hand. In an attempt to separate the altered mixing noise from the propagation effects, a solution might be to apply the methodology suggested by Stephens and Morris [34] and generalized by Pasco and Moreau [35] for low speed ducted fans. In these applications, the global noise of the whole system is not only generated by the rotor itself (the sound source) but is also combined with the acoustic disturbances induced by the surfaces surrounding the source like the fan casing. In order to dissociate these two contributions, the radiated sound has been described as the product of a source function based on a flow velocity for a given Strouhal number and a transfer function accounting for all the propagation effects. The departure of the measured sound power level from the power law for a given Strouhal number is then attributed to perturbations caused by acoustic propagation in the presence of the surrounding surfaces. A similar technique has also been proposed by Zhang et al. [36] for confined turbulent jets.

A similar decomposition is applied to the present measurements. Indeed, it has been observed in Fig. 9, that the resonance frequencies remain relatively constant when the NPR increases suggesting a weak effect of the mean flow in the output duct on to the acoustic propagation from a frequency point of view. It will thus be assumed that the far-field spectra (Π) can be decomposed into a source part (Ψ), induced by the jets issuing from the plates and evolving according to an unknown velocity power law for a given Strouhal number, and a propagation part (H) that takes into account all perturbations due to the propagation through the output duct. The latter is obtained from the ratio between the total sound power and the source function *i.e.* $H = \Pi/\Psi(St, M_j)$ with:

$$\Psi = \Psi_0(St) M_j^{n(St)}. \tag{12}$$

where M_j is the jet Mach number (Eq. (7)) and n a real number. The logarithm of Π thus writes:

$$\log(\Pi) = \log(H) + \log(\Psi_0(St)) + n(St)\log(M_j). \tag{13}$$

The measurements made for various operating points are then used to determine the velocity power law of the source (Ψ_0 and n) for a given Strouhal number by linear regression. The deviations from this power law in the frequency domain are thus attributed to the propagation effects. In the present case, only low supersonic regimes are investigated. Therefore, both subsonic and supersonic NPRs are compared with the same power law [19,37,38]. The Strouhal number is based on the perforation diameter D.

The decomposition algorithm is applied to the diaphragm S1 as well as to the perforated plate S1D3N3e3 in Figs. 11 and 12 for $\Theta = 90°$ and $30°$ respectively. Figs. 11(a) and 12(a) are devoted to S1 whereas Figs. 11(b) and 12(b) display the results obtained with S1D3N3e3. For each case, the sound pressure level measured by the microphone Π, the acoustic transfer function of the duct H and the acoustic source associated with the mixing noise Ψ are plotted from top to bottom respectively. As expected, for both angles, the acoustic transfer function contains all the modulations that appear when the output duct is added to the free jet configuration [1] and that have been identified as longitudinal resonances and duct modes in Sec. 4. The predicted frequencies of the longitudinal resonances (Eq. (6)) and the first two azimuthal modes (Eq. (5)) are highlighted by the black dashed and solid lines respectively in Figs. 12 and 11. Note that for this prediction, the vena constracta effect is assumed to be similar in both the diaphragm and the perforated plate cases, which is probably not perfectly right but offers satisfactory predictions. The obtained transfer function H is consistent with the modelling reported in Ref. [9]. The source spectra Ψ are now smoother and some characteristics of the mixing noise observed without outlet duct [1], can already be recognised. For instance, a perforated plate with widely spaced perforations (S1D3N3e3) increases the high frequency sound due to a delayed merger of the jetlets with respect to the diaphragm or to closer spaced perforations [1]. Note however that some modulations persist in the source spectrum of S1D3N3e3. These are mainly due to the limited number of NPRs that are available for the regression, but also to the intense resonances found in this case that may locally modify the calculated power law.

Once the duct contribution is separated from the noise source itself, the mixing noise generated by the discharge though the plates in this confined configuration can be analysed.

6. Study of the mixing noise

6.1. Overall results

Without duct [1], the mixing noise generated by the flow through a diaphragm was first shown to have very similar characteristics (spectral shapes, characteristic frequencies, levels) to those of a jet issuing from more conventional nozzles. For

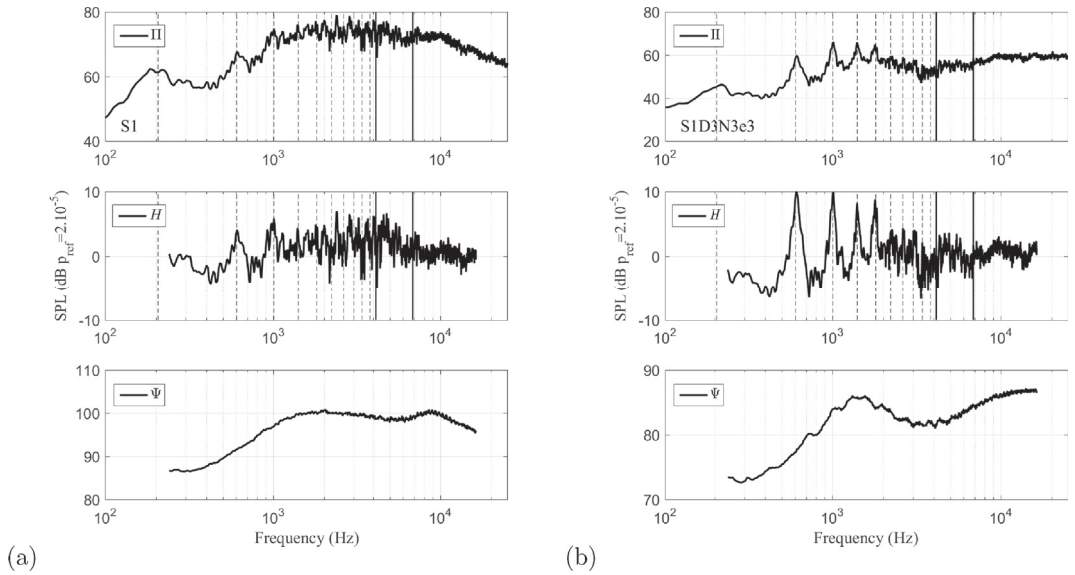

Fig. 11. Source decomposition [34,35] applied to: (a) diaphragm S1, and (b) perforated plate S1D3N3e3 for NPR = 2 and $\Theta = 90°$. The dashed black lines are the predicted longitudinal resonance frequencies given by Eq. (6) and the solid black lines are the cut-on frequency of the first two azimuthal modes given by Eq. (5).

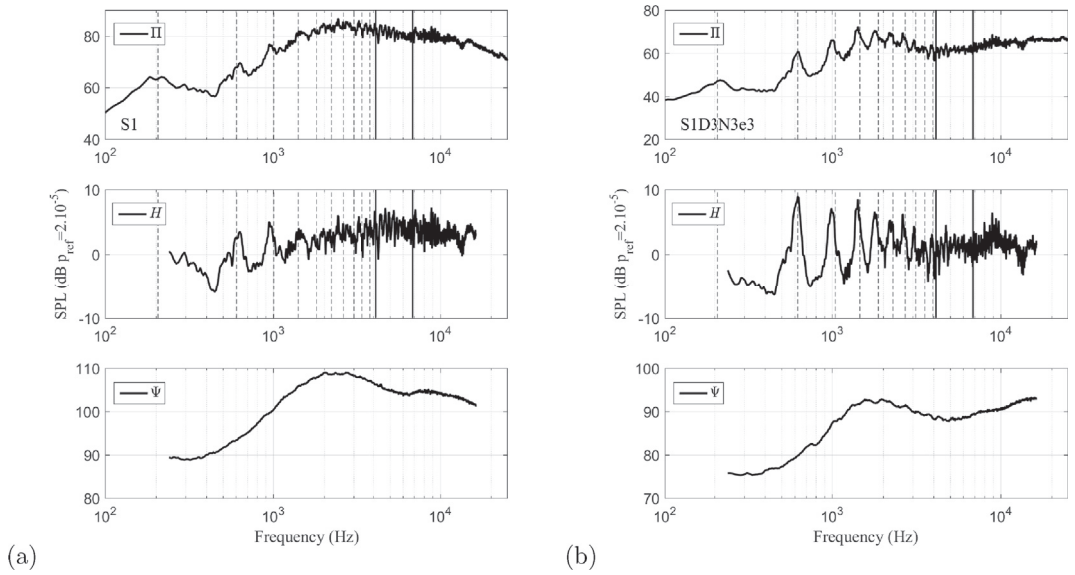

Fig. 12. Source decomposition [34,35] applied to: (a) diaphragm S1, and (b) perforated plate S1D3N3e3 for NPR = 2 and $\Theta = 30°$. The dashed black lines are the predicted longitudinal resonance frequencies given by Eq. (6) and the solid black lines are the cut-on frequency of the first two azimuthal modes given by Eq. (5).

the perforated plate case however, the mixing noise was composed of two humps associated with distinct zones of the jet development. To briefly summarize the main findings in Ref. [1], the high frequency hump has been associated with the radiation of the individual small jets issuing from the perforations while the low frequency hump is attributed to the mixing of the large equivalent jet formed downstream of the merger of all individual small jets. Based on these results, it is possible to adapt the mixing noise of the perforated plates by favoring or not the rapid mixing of the jetlets. For example, in the case of a perforated plate with widely spaced perforations, the mixing of the individual small jets is delayed with respect to configurations with closer perforations and the associated radiation therefore enhances the high frequency noise and reduces the low frequency noise.

By now adding a duct downstream of the perforated plates or diaphragms, the interaction of the jet shear layers with the duct walls or with the acoustic field is likely to modify the mixing noise. Indeed, according to Laffite [39], the potential core for a confined jet is longer than that of an equivalent free jet. The turbulence development also stretches over a much longer

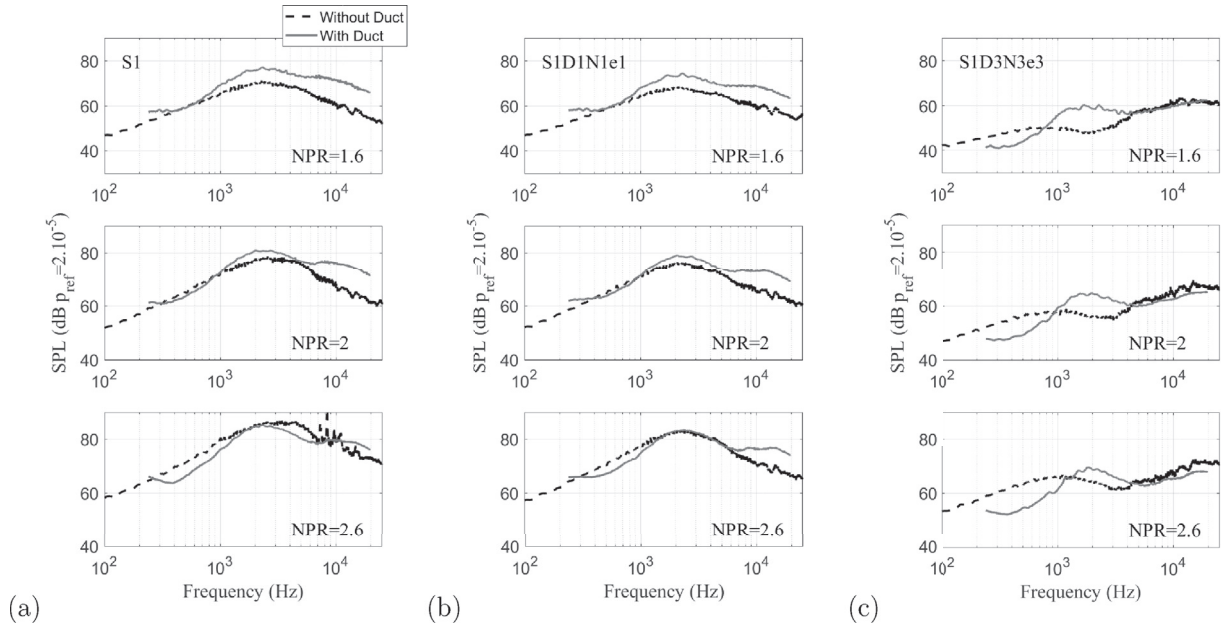

Fig. 13. Comparison of the mixing noise with and without duct at $\theta = 30°$ for: (a) diaphragm S1, (b) perforated plates S1D1N1e1 and (c) S1D3N3e3.

distance and the mean velocity on the jet axis increases. This author also observed a strong modification of the radiated far-field noise with a smaller power law exponent and a modified maximum amplitude frequency.

Figs. 13 and 14 compare the mixing noise obtained at $\Theta = 30°$ and 90° respectively in the configuration without duct and with duct for two perforated plates and the associated diaphragm as well as three operating points. The three plate geometries have the same total perforation area.

First, for the three configurations at $\Theta = 30°$ (Fig. 13), the sound level significantly increases when the output duct is added for NPR = 1.4. With increasing NPRs, this sound amplification gradually weakens down to an attenuation for NPR = 2.6. The evolution of the radiated sound power level as a function of the operating point thus seems to be modified by the duct. For S1 and S1D1N1e1, the spectral shapes remain relatively similar in both configurations despite a slight increase of the high

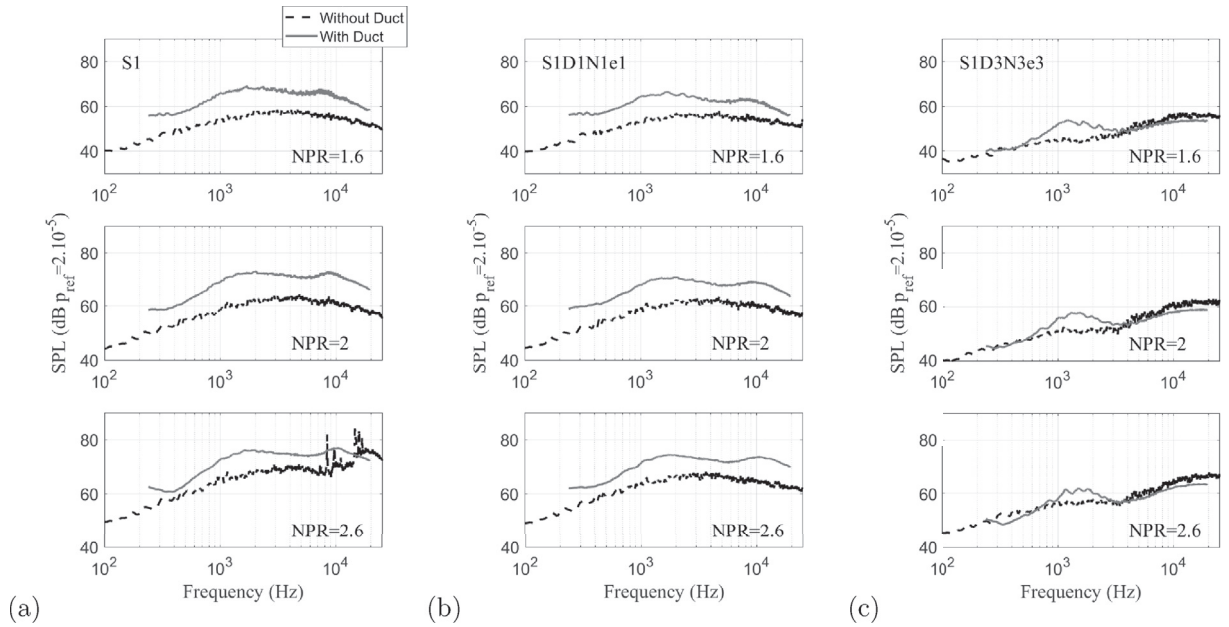

Fig. 14. Comparison of the mixing noise with and without duct at $\theta = 90°$ for: (a) diaphragm S1, (b) perforated plates S1D1N1e1 and (c) S1D3N3e3.

frequencies as well as a decrease of the low frequencies when the duct is added. For the perforated plate S1D3N3e3 that is composed of the most spaced perforations, the spectra are strongly modified in particular at low and medium frequencies. Indeed for this case, the high frequency hump seems well preserved when the outlet duct is added while the low frequency hump is slightly shifted towards higher frequencies. Because of this shift, the low frequencies strongly decrease. For the three geometries, the maximum amplitude of the low-frequency hump is seen to appear approximately at $f = 2000$ Hz for NPR $= 1.4$. This suggests that a common dimension seems to drive the frequency domain of this low frequency hump for the three geometries. This common dimension is likely to be the duct diameter that corresponds to the diameter of the fully developed output jet.

The results for $\Theta = 90^\circ$ are shown in Fig. 14. The acoustic gap between the two configurations is more important for plates S1 and S1D1N1e1 than for S1D1N1e3, even though it also decreases as the NPR increases. As noted in Sec. 3, the widening of the spectra, typical of the jet mixing noise when turning from downstream to sideline directions, is naturally less pronounced in the ducted configuration. Indeed, the presence of the duct modifies not only the sources but also the directivity of the jets at the exit of the perforated plates. For plate S1D3N3e3, similar observations as for $\Theta = 30^\circ$ can be made. Finally for the three plates, the maximum amplitude of the low frequency hump occurs at a slightly lower frequency on the sideline directions ($\Theta = 90^\circ$) compared with the downstream direction in the ducted configuration. For the free jet, the shift is opposite which is in agreement with jet mixing noise theory [18,19,38].

In the following subsection, a more detailed analysis of the mixing noise from the diaphragms and perforated plates in the presence of the outlet duct is carried out.

6.2. Diaphragms

First of all, the diaphragm cases are discussed. It has been observed in the previous comparisons that the output duct modifies the broadband noise level as well as the shape of the spectra. In order to further study this noise component, the source function Ψ extracted from the decomposition algorithm for the diaphragm S1 at different NPRs, is plotted as a function of the Helmholtz number $He = \frac{fD_d}{c_0}$ based on the output duct diameter D_d in Fig. 15 (a) and (b) for $\Theta = 90^\circ$ and 30° respectively. Modifications of the mixing noise can be observed compared to the free jet [1]. Indeed, the mixing noise generated by a free jet is characterized by a single hump which tends to flatten and widen in the downstream directions. This modification of the mixing noise spectra is associated with the dominant radiation of large coherent turbulent structures in the downstream directions and of the fine scale turbulence in the sideline directions. Moreover, for the free jet, the maximum amplitude of the mixing noise is characterized by a fairly constant Strouhal number St, based on the jet diameter and velocity, and its value changes from approximately 0.2 to 0.3 from the downstream to the sideline directions [19,38,40,41]. Although it is less pronounced than in the free jet configuration (Fig. 13 (a)), the shape of the mixing noise spectrum also changes in the ducted

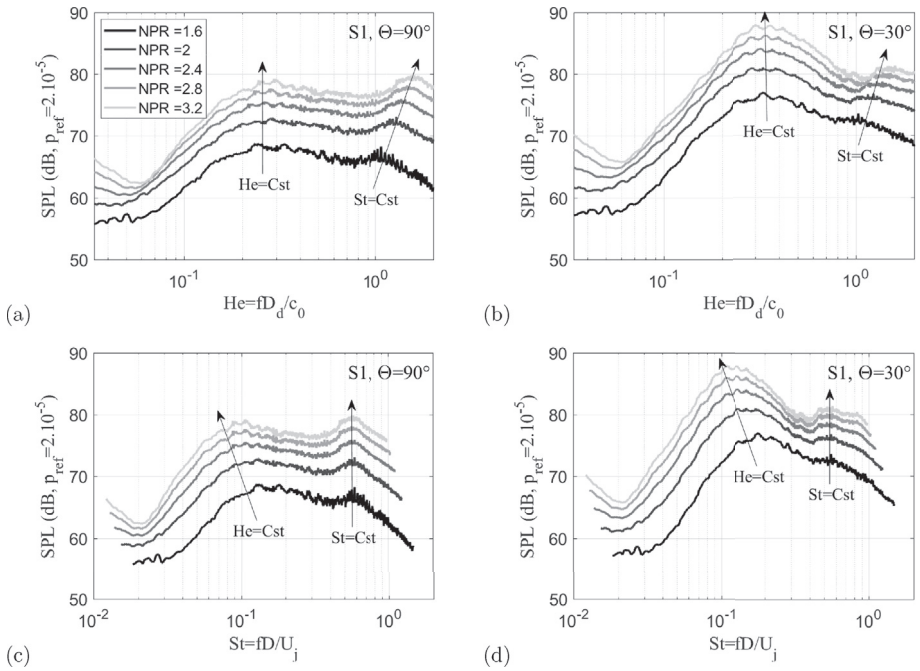

Fig. 15. (a), (b) Extracted broadband noise as a function of He for diaphragm S1 at $\Theta = 90^\circ$ and 30° respectively. (c), (d) Extracted broadband noise as a function of St for diaphragm S1 at $\Theta = 90^\circ$ and 30° respectively.

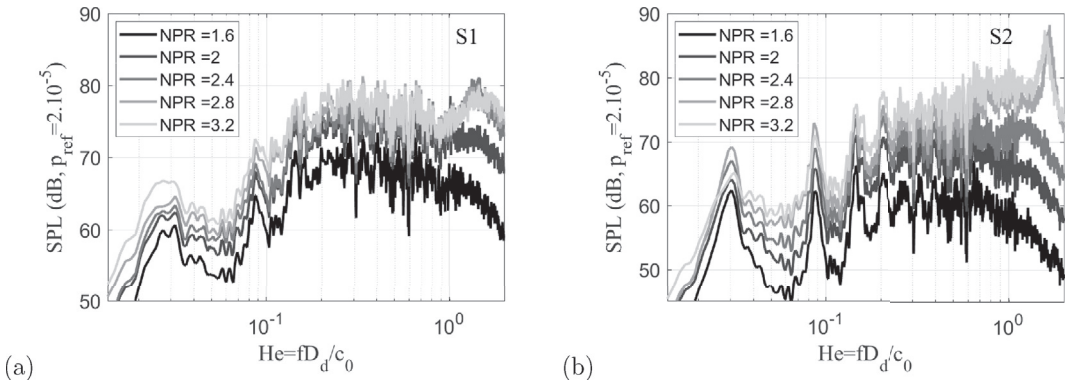

Fig. 16. (a), (b): Raw spectra as a function of *He* at $\Theta = 90°$ for diaphragms S1 and S2 respectively.

case between $\Theta = 30°$ and 90°. However the Helmholtz number of the maximum amplitude does not depend on the NPR: its value is typically about 0.25 at 90° and 0.33 at 30°, whereas the associated Strouhal number is of course not constant. In addition a second hump can be recognised at a constant Strouhal number $St \simeq 0.55$ for $\Theta = 90°$ and 30° as shown in Fig. 15(c) and (d).

In order to analyze this high frequency hump, the raw spectra without decomposition is presented in Fig. 16. Fig. 16 (a) shows that the high frequency hump appears for all operating points for S1 whereas it cannot be distinguished for the subsonic NPR (= 1.6) for the S2 diaphragm (Fig. 16 (b)). Obviously several phenomena contribute to this hump. Among these are: BBSAN, influence of the duct onto the shock cells and propagation effects (duct modes). In Fig. 15, the decomposition algorithm smooths this hump for supersonic regimes. The slight jump that can be observed at high frequency on the raw spectra for subsonic NPRs is most likely related to the apparition of the second azimuthal acoustic mode (see Sec. 4).

As shown by Lighthill [3], the noise produced by a turbulent jet is dominated by quadrupolar sources that explain the U_j^8 velocity dependance of the sound power (in fact experimental evidence shows that the evolution of the sound intensity is closer to U_j^9 in the downtream direction and to $U_j^{7.5}$ in the sideline direction due to convection effects [1,37,38]). However in the case of a ducted jet as in the present application, several studies have shown that the noise inside the duct is dominated by dipolar sources. These are induced by interactions between the turbulent flow inside the duct and edges that lead to a modification of the sound power law [42,43]. This result might explain why the NPR dependance and the directivity of the noise level change between the ducted and free configurations shown in Figs. 13 and 14. In order to determine the power law in the ducted configuration, the maximum amplitude of the lower frequency hump (hereafter referred to as the main hump) is plotted in Fig. 17 for the diaphragm S1 as a function of the perfectly expanded Mach number (Eq. (7)). For this diaphragm, the maximum amplitude of the main hump appears at a lower frequency than the cut-on frequency of the first azimutal mode ($f_{c_{1,1}} = 4136$ Hz), which means than only the plane mode propagates. In both directions (30° and 90°) an evolution according to a fifth power law is observed, which corresponds quite well with the radiation of dipolar sources outside a hard wall duct as observed by Nelson and Morfey [42]. Note that this power law is determined for a constant frequency or Helmholtz number

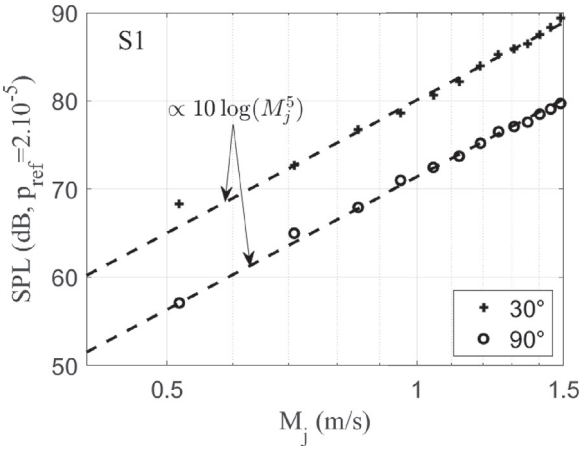

Fig. 17. Evolution of the amplitude of the maximum of the low-frequency hump as a function of the operating point for diaphragm S1.

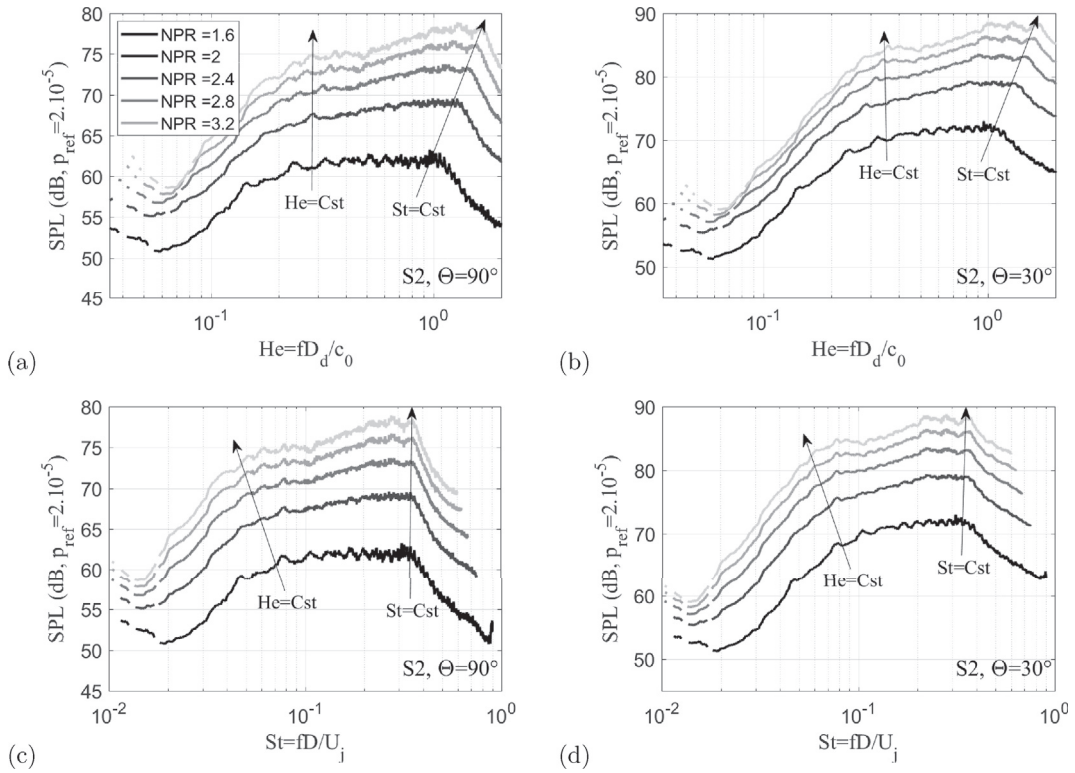

Fig. 18. (a), (b) Extracted broadband noise as a function of *He* for diaphragm S2 at $\Theta = 90°$ and 30° respectively. (c), (d) Extracted broadband noise as a function of *St* for diaphragm S2 at $\Theta = 90°$ and 30° respectively.

and not for a constant Strouhal number. This result can also explain the noise level gap between the two configurations observed in Fig. 13 (a) and 14 (a) as a function of the NPR and observation angle. Indeed, for diaphagm S1 and $\Theta = 30°$ the power law of the main hump varies from Uj^9 in the free configuration [1] to U_j^5 in the ducted one, while for $\Theta = 90°$, it varies from $U_j^{7.5}$ to U_j^5.

A similar analysis is now achieved for the smallest diaphragm S2 in Fig. 18. Two humps can be observed as for S1. The maximum amplitude of the low frequency hump does not vary with frequency when the NPR increases. Again it does not appear for a constant Strouhal number based on the jet velocity as it does for the free jet but for a constant Helmholtz number based on duct diameter ($He \simeq 0.28$ at 90° and 0.34 at 30°). For this diaphragm as well, a high frequency, constant Strouhal hump appears around $St \simeq 0.35$ at supersonic NPRs in the far-field spectra (Fig. 16 (b)) and in Fig. 18 (broadband noise extractions). This hump is probably due to several contributions (BBSAN and duct propagation effects); however, the aerodynamic flow/duct interactions are likely to be much weaker in this case than in the S1 case, since the diameter of the diaphragm S2 is almost 4 times smaller than the duct diameter.

In Fig. 19, the SPL of the maximum amplitude of the low frequency hump is plotted as a function of the Mach number. As for the *S*1 diaphragm, this hump also appears below the cut-on frequency of the first azimutal mode so that only the plane mode propagates. The amplitude grows with the 6.5th power of the perfectly expanded Mach number, which again is consistent with the work of Nelson and Morfey [42].

6.3. Perforated plates

Fig. 20 shows the broadband noise spectra for S1D1N1e1 and S1D2N2e3 at different operating points and at $\Theta = 30°$ and 90°. As in the free case [1], the dual hump characteristic of the perforated plate mixing noise appears. Indeed, unlike for diaphragm cases, the high frequency hump clearly appears for all NPRs and is thus not caused by shock noise, as shown in Fig. 4. However, the variation of the hump level and frequency range are slightly different from those of the free configuration. Indeed, as for the diaphragms, the frequency at which the low frequency hump maximum amplitude appears, does not significantly vary with the NPR ($\Theta = 30°$ (Fig. 20 (a) and (b)): $He \simeq 0.34$ for S1D1N1e1 and 0.29 for S1D3N3e3), while the maximum of the high frequency hump is obtained for an approximately constant Strouhal number based on the perfectly expanded jet velocity and perforation diameter ($\Theta = 90°$ (Fig. 20 (c) and (d)): $St \simeq 0.22$ for S1D1N1e1 and 0.23 for S1D3N3e3).

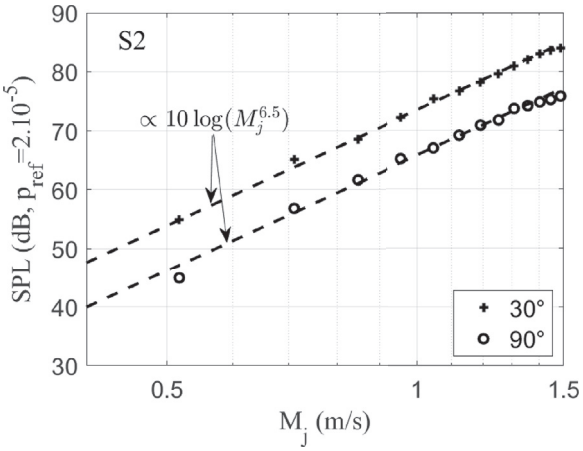

Fig. 19. Evolution of the maximum amplitude of the low frequency hump as a function of the operating point for diaphragm S2.

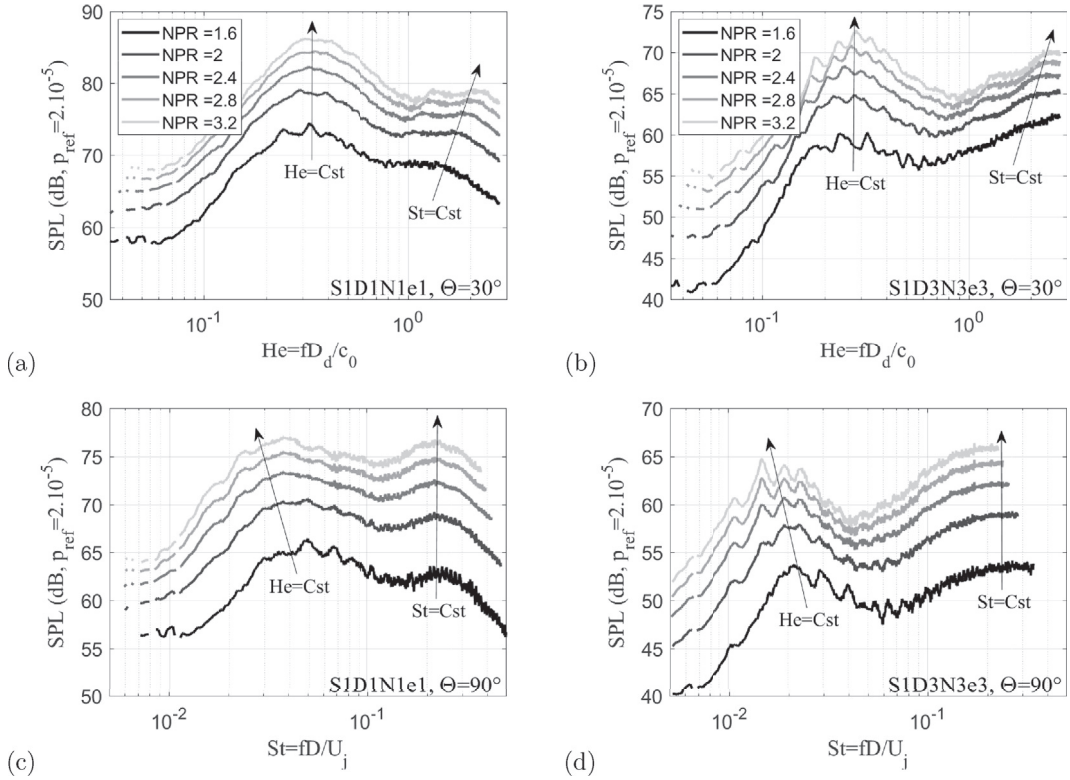

Fig. 20. Extracted broadband noise as a function of *He* at $\Theta = 30^\circ$ for perforated plates S1D1N1e1 (a) and S1D3N3e3 (b). Extracted broadband noise as a function of *St* at $\Theta = 90^\circ$ for perforated plates S1D1N1e1 (c) and S1D3N3e3 (d).

The latter result is consistent with the assumption that the high frequency hump is generated by the mixing of the small jets exiting from the perforations of the plate.

As was done in the unducted case [1], the evolution of the far-field sound as a function of perforated plate geometry is studied in Fig. 21 for NPR = 2 and $\Theta = 30^\circ$. All the perforated plates presented in these spectra have the same total perforation area but various perforation diameters and spacings.

In Fig. 21 (a) and (c), the mixing noise for perforated plates with same cross-section *S*, perforation diameter *D* and number *N* but different perforation spacing *e*, is plotted against the Helmholtz number. Again, significant modifications can be observed in the ducted configuration compared with the free one. In the free jet configuration, it was found that increasing *e* (Fig. 6 in Ref. [1]) increases the amplitude of the high frequency hump (merging hump) and reduces the amplitude and the

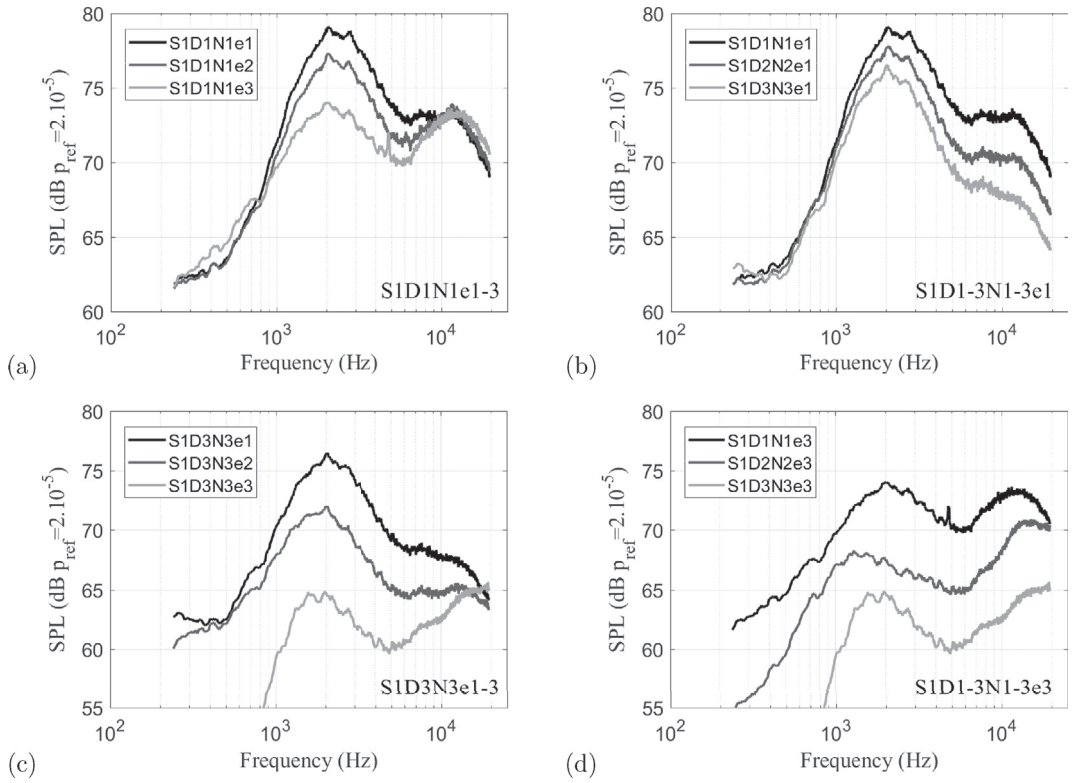

Fig. 21. Extracted broadband noise as a function of perforated plate geometric parameters at $\Theta = 30^{\circ}$ and NPR = 2 for: (a),(c): perforated plates with different perforation spacing, S1D1N1e1-3 and S1D3N3e1-3 respectively; (b), (d): perforated plates with different perforation diameter and number, S1D1-3N1-3e1 and S1D1-3N1-3e3 respectively.

frequency of the low frequency hump (post-merging hump). Indeed, as explained in Ref. [1], this is due to the fact that the small jets behave more as independent small jets if their spacing increases whereas their merger is shifted downstream; therefore the resulting large jet is wider and its mixing weaker when the perforation spacing increases. In the present ducted configuration, the low frequency hump is also considerably reduced when e increases. This decrease is even stronger when the diameter of the perforations is reduced (S1D3N3e1-3). The ratio e/D therefore seems to be the dominant parameter governing the level of the low frequency hump. In order to verify this assumption, the evolution of the amplitude of the low frequency hump maximum (SPL_{max}) is plotted against e/D in Fig. 22 (a) for all tested perforated plates with a total perforation area S =S1 and for different NPRs. The maximum amplitude of the low frequency hump varies linearly with the ratio e/D for all NPRs. The slope is approximately -14.3 dB per unit e/D for the configurations with an overall cross-section S1. The y-intercept however increases with the operating point (NPR). Its evolution in Fig. 22 (b) follows a power law of M_j given by: $10\log(KM_j^{6.5})$ with $K = 7.1 \times 10^7$ for the present configurations. The Mach number exponent 6.5 yielding the sound pressure level of the low frequency hump is again consistent with the work of Nelson and Morfey [42]. Note that this power law is defined for a constant Helmholtz number but not a constant Strouhal number. Finally by combining these two results, it is possible to determine a global empirical law predicting the maximum amplitude of the low frequency hump for all the present perforated plates with cross-section S1 and all operating points at $\Theta = 30^{\circ}$. To do so, the maximum amplitude of the low frequency hump is normalized by the previously determined power law yielding a normalized level (SPL_{norm}) *i.e.*: $SPL_{norm} = SPL_{max} - 10\log(KM_j^{6.5})$. The results are synthesized in Fig. 22 (c) into a single linear normalized maximum amplitude according to the following law:

$$SPL_{norm}(dB) = -14.3e/D. \tag{14}$$

Still by increasing the perforation spacing for a constant diameter (Fig. 21(a) and (c)), it can also be noticed that unlike in the unducted case [1], the frequency of the maximum of the low frequency hump does not vary. This suggests that a constant dimension governs this positioning for the perforated plates S1D1N1e1-3 but also S1D3N3e1-3. The geometrical parameters of these plates being very different (circumscribed diameter, perforation diameter, number and spacing), it can be expected that the common dimension is the size of the outlet duct. Indeed, the output duct limits the development of the downstream jet formed by the merger of all the individual small jets and that is responsible for the low frequency hump as in the free

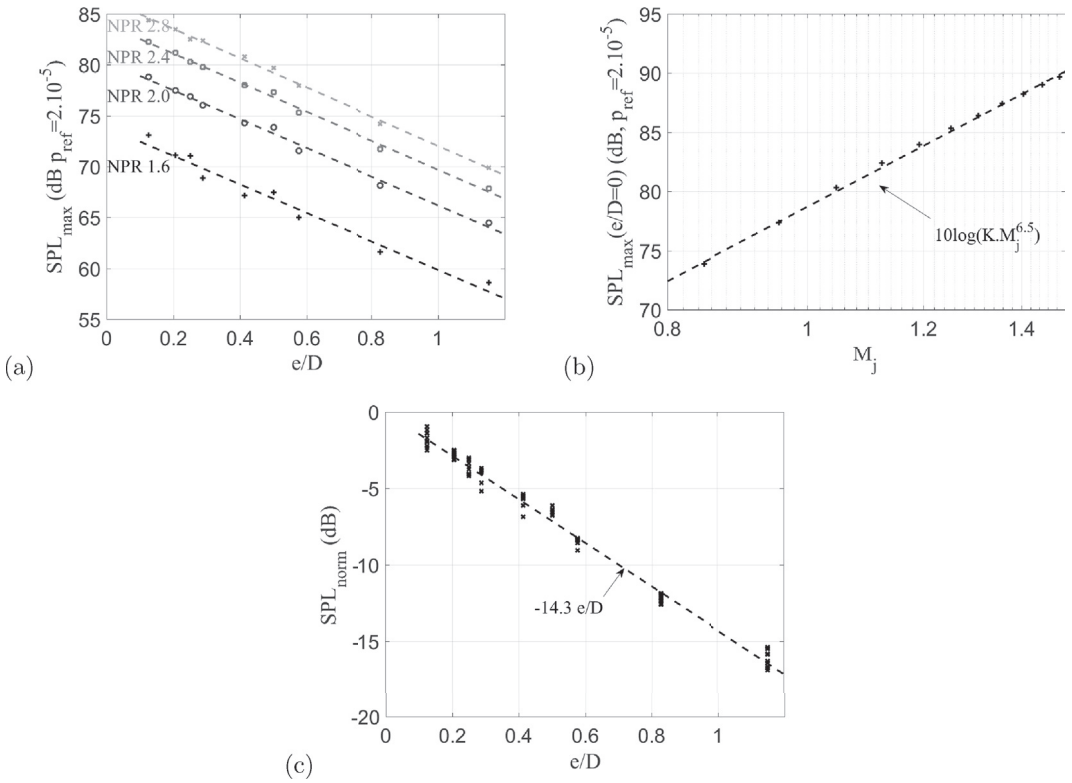

Fig. 22. (a) Evolution of the low frequency hump maximum amplitude as a function of the ratio e/D for all perforated plates with cross-section S1. (b): Evolution of the low frequency hump maximum amplitude as a function of the perfectly expanded Mach number for all perforated plates with cross-section S1. (c) Global evolution of the maximum amplitude of the low frequency hump normalized by the perfectly expanded Mach number as a function of the ratio e/D for all perforated plates with cross-section S1.

configuration [1]. The high frequency hump however is less affected by the increase of the perforation spacing as shown in Fig. 21 (a) and (c). For the perforated plates S1D1N1e1-3, the level of this hump is maintained while for S1D3N3e1-3, only a slight reduction can be observed. The flow mixing at the exit of the perforated plates is significantly influenced by the duct as it bounds the mixing within the duct section.

By now decreasing the perforation diameter D and increasing the perforation number N (to maintain a constant cross-section) for a constant perforation spacing e (Fig. 21 (b) and (d)), a reduction of the two hump levels can again be observed but this time in a uniform way for both humps. In fact, the reduction of D and the increase of N for a constant e only reduces the overall level of the radiated spectrum.

At first glance, for the above mentioned reasons, the peak frequency of the low frequency hump remains fairly constant, except for S1D2N2e3 that is shifted to lower frequencies. So far, no explanation has been found for this particular shift that requires additional flow measurements and visualizations. For the high frequency hump, two behaviors can be observed depending on the spacing. For large spacings ($e3$), the peak frequency of the high frequency hump decreases when the perforation diameter increases, which is consistent with jet noise theory applied to each individual perforation. Conversely, for small spacing ($e1$), the peak frequency remains fairly constant when the perforation diameter varies, which is surprising as it apparently contradicts classical jet noise results. Although no firm scenario has been found to explain this observation, it is very likely that the shear layers of neighboring “jetlets” interact strongly enough to rule out the isolated jet mixing mechanisms: thus the frequency would rather scale with $e1$ than with the jetlet diameters $D(1..3)$ when the spacing is very small compared to the diameters. As a result, the frequency dependence of the high frequency hump would be a governed by the parameter e/D.

7. Study of the shock noise

Finally, the last sound component that remains to be studied is that of the strong low frequency lines appearing at supersonic operating points for the largest diaphragm S3 (Fig. 4 (d)) and perforated plates S3D2N3e1 and S4D4N4e1. For these configurations, the far-field acoustic spectra are not strongly influenced by the modulations of the broadband noise due to acoustic duct resonances and can therefore be analysed directly.

Several studies have already been conducted both numerically and experimentally on the aeroacoustic phenomena that appear when a transonic flow passes through a sudden duct section expansion [5–8,44]. They have shown the emergence of different regimes depending on the NPR that may be responsible for a significant acoustic radiation. Similar mechanisms might explain these strong low frequency lines.

In the case of a duct with a rectangular cross-section, Anderson et al. [6] observed for the highest NPR, a series of oblique shock cells along the entire length of the output duct downstream of the sudden expansion (Fig. 23 (a)). This oblique shock pattern is stable. It shortens as the NPR decreases and the downstream end of the shock cells comes closer to the plate. The behavior then becomes unstable due to the random distortion of the shock-wave pattern induced by the turbulent jet. This phenomenon causes non-periodic pressure oscillations at the outlet of the duct (Fig. 23 (b)). By further reducing the NPR, the flow becomes again unstable as it transitions from oblique shocks to a single normal shock (Fig. 23 (c)). Indeed during a cycle of this oscillating regime, the shock structure switches from oblique to normal patterns. When the NPR is further reduced, the regime becomes stable with a single normal shock at the exit of the expansion (Fig. 23 (d)). This shock reaches the walls of the outlet duct so that, in the same way as for the previous cases, supersonic flow regions are attached to the duct walls and no acoustic disturbance can reach the upstream corners. However, if the pressure ratio is futher reduced, the intensity of the normal shock decreases and no longer reaches the duct walls (Fig. 23 (e)). As a result, the flow becomes subsonic near the duct wall and upstream of the shock between the core flow and the walls, allowing acoustic waves to travel in the upstream direction to the perforated plate. Since the normal shock oscillates, strong pressure oscillations can appear at the corners of the expansion that are no longer “no-flow regions” and generate an unstable regime named “base pressure oscillations”. This regime can also appear in the case of a cylindrical duct [5,6]. The self-exciting mechanism of these base pressure oscillations is irregular but can sometimes be locked on the longitudinal resonance frequencies of the outlet duct generating a strong coupling and powerful sound waves. This might explain the intense tones that appear for the diaphragm S3 as well as for the perforated plates S3D2N3e1 and S4D4N4e4 in the range $2.4 \leq \text{NPR} \leq 3.4$ corresponding to the lower NPRs in the experiment of Anderson et al. [6].

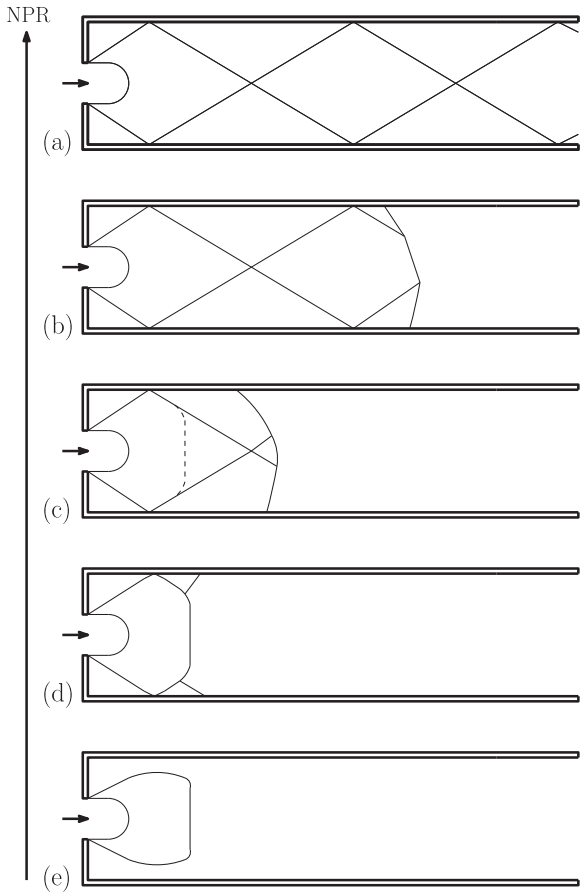

Fig. 23. Sketch of the different aerodynamic regimes appearing downtream of a sudden section expansion in the case of a rectangular duct according to Anderson et al. [6].

This phenomenon has also been addressed numerically by Emmert et al. [44] who showed that the fundamental frequency f_0 of this noise mechanism is locked on the first longitudinal resonance of the output duct while other radiated frequencies are harmonics of this fundamental frequency. In Fig. 24 the experimental spectra of S0, S3D2N3e1 and S4D4N4e4 are plotted at the operating points for which the low frequency lines appear. In these spectra the fundamental frequency (lowest frequency line), named f_0, is given by the solid black line while the dashed lines give the first harmonics of this fundamental frequency. As observed by Emmert et al. [44], an excellent agreement between these different frequencies and the lines in the spectra is obtained, suggesting the presence of the base pressure oscillations in the present configurations.

Moreover, the measured fundamental frequencies are reported in Table 3 as a function of the NPR for the three configurations. For diaphragm S3 and NPR $\leq$2.6, a fairly good agreement between the measured fundamental frequency and the first longitudinal resonance frequency given by Eq. (6) ($f_{r_1} = 187$ Hz at NPR = 2.4 and 184 Hz at NPR = 2.6) can be seen. This has also been observed by Emmert et al. [44]. The slight differences may result from the approximations made for the calculation of the average Mach number in the output duct. When the NPR is increased, a jump of the fundamental frequency is observed. These higher frequencies seem to correspond to multiples of the first longitudinal resonance frequency and may be explained by an overblowing phenomenon as observed on wind instruments. For the two perforated plates S4D4N4e4 and S3D2N3e1, fundamental frequencies are of the same order as for S3 (NPR $\leq$ 2.6) suggesting a similar mechanism. Again, the minor differences that appear between the plates probably result from some variation of the mean flow that depends on the cross section and the associated vena contracta effect.

Finally, when the NPR is increased above the range presented in Fig. 24, all lines as well as modulations due to the longitudinal resonances are totally suppressed. According to the regimes introduced in Fig. 23, it can be inferred that the normal shock has an increased intensity and reaches the duct walls. Supersonic regions are then attached to the duct walls. As a result there are no longitudinal modes and no feedback anymore, thus suppressing the modulations and lines in the spectra.

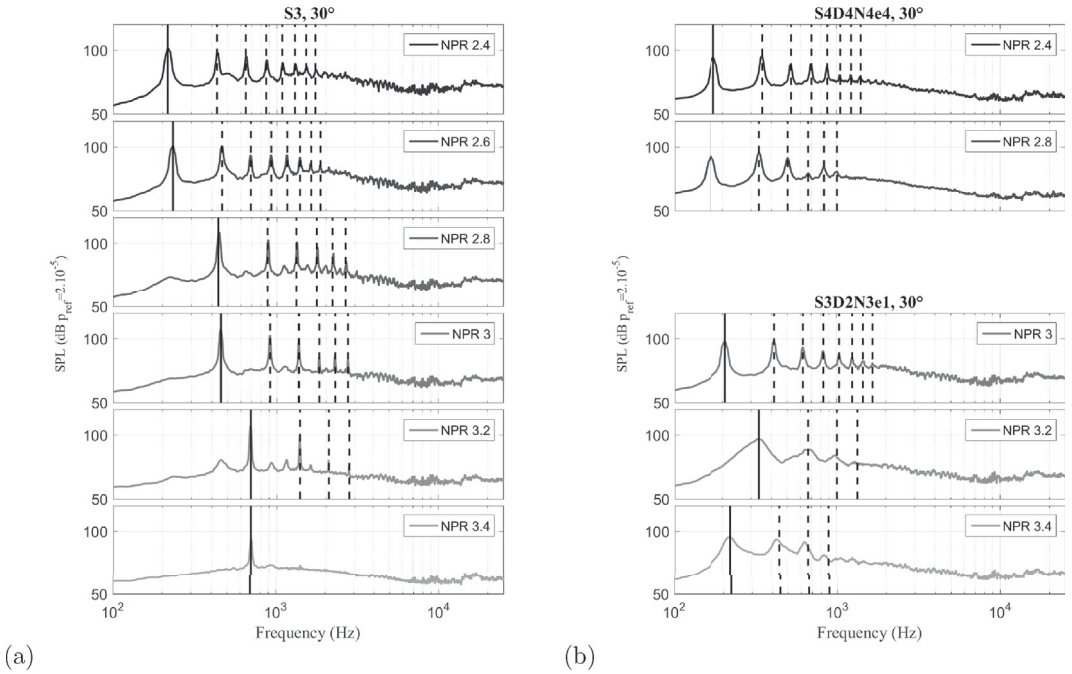

Fig. 24. Comparison of the far-field acoustic measurements with the predicted frequencies of the base pressure oscillations at $\Theta = 30°$ for: (a) diaphagm S1 and (b) perforated plates S4D4N4e4 and S3D2N3e1. The continuous black lines give the experimental fundamental frequency (f_0) of the base pressure oscillations and the dashed lines the harmonics ($n \times f_0$).

Table 3
Fundamental frequency f_0 of the base pressure oscillations as a function of the NPR for configurations S3, S4D4N4e4 and S3D2N3e1.

	S3						S4D4N4e4		S3D2N3e1		
NPR	2.4	2.6	2.8	3.0	3.2	3.4	2.4	2.8	3	3.2	3.4
f_0 (Hz)	216	232	440	456	696	696	176	168	208	336	224

8. Conclusion

An experimental study of the noise generated by a ducted air flow discharge through diaphragms and perforated plates has been conducted and is compared to the noise radiated by the same discharge in a free environment [1].

As expected the mixing noise is strongly modified by the output duct that generates acoustic longitudinal resonances and duct modes leading to strong modulations of the broadband noise. In particular, the perforated plate geometry is shown to have an effect on the emergence of these modulations.

In order to extract the aerodynamic part of the source from all other sound and flow-sound interactions due to the duct, a decomposition technique from the literature has been applied. This allowed to highlight the similarities and differences between the ducted and unducted configurations and confirmed the important role of the plate geometry in the far field radiation.

In particular the far field spectra for perforated plates are dominated by two humps. The maximum level of the dominant hump (low frequency hump) grows linearly (in dB) with the ratio of the perforation diameter to their mutual spacing and its frequency is observed at a constant Helmholtz number instead of a constant Strouhal number found in the unducted case. This suggests that in the ducted case, the frequency is governed by a flow-sound interaction, but the underlying physical mechanism has not yet been identified. Moreover, the level of this peak value is found to vary as ($\sim U^5$ - $\sim U^6$) [39,42,43,45,46] instead of ($\sim U^8$) in the unducted case. As a result, the ducted case is louder at low NPRs.

For the high frequency hump, the frequency of its peak value is observed at a constant Strouhal number as for the unducted case. Its level does not depend on the perforation spacing but it emerges more for large spacings since the jetlets interact further downstream with each other. As expected, its level increases with the perforation size as the jetlets become louder. Thus, the level is a function of the parameter e/D.

Finally, for diaphragms, at supersonic operating points, the screech radiation observed in the free-field case is suppressed but the broadband shock associated noise remains in the high frequency range. For largest diaphragms and perforated plates, strong low frequency lines are found at high NPRs. These lines are caused by a coupling between shocks and longitudinal resonances and are locked on a series of harmonics.

Acknowledgements

This work was performed within the framework of the Labex CeLyA of the Université de Lyon, within the programme "Investissements d'Avenir" (ANR-10- LABX-0060/ANR-16-IDEX-0005) operated by the French National Research Agency (ANR) and is also supported by the industrial Chair ADOPSYS co-financed by Safran Aircraft Engines and the ANR (ANR-13-CHIN-0001-01). Authors also acknowledge Prof M. Roger and Dr Y. Pasco for fruitful discussions.

References

[1] P. Laffay, S. Moreau, M. Jacob, J. Regnard, Experimental study of the noise radiated by an air flow discharge through diaphragms and perforated plates, J. Sound Vib. 434 (2018) 144–165.
[2] H. Davies, J. Ffowcs Williams, Aerodynamic sound generation in a pipe, J. Fluid Mech. 32 (4) (1968) 765–778.
[3] M. Lighthill, On sound generated aerodynamically. I. General theory, Proc. R. Soc. Lond. 211 (1107) (1952) 564–587.
[4] M. Lighthill, On the sound generated aerodynamically. II. Turbulence as a source of sound, Proc. R. Soc. Lond. 222 (1148) (1954) 1–32.
[5] J. Anderson, T. Williams, Base pressure and noise produced by the abrupt expansion of air in a cylindrical duct, J. Mech. Eng. Sci. 10 (3) (1968) 262–268.
[6] J. Anderson, W. Jungowski, W. Hiller, G. Meier, Flow oscillation in a duct with a rectangular cross-section, J. Fluid Mech. 79 (4) (1977) 769–784.
[7] G. Meier, G. Grabitz, W. Jungowski, K. Witczak, J. Anderson, Oscillations of the supersonic flow downstream of an abrupt increase in duct cross section, AIAA J. 18 (4) (1980) 394–395.
[8] G. Meier, P. Szumowski, W. Selerowicz, Self-excited oscillations in internal transonic flows, Prog. Aerosp. Sci. 27 (1990) 145–200.
[9] P. Laffay, M. Jacob, S. Moreau, J. Regnard, Experimental investigation of the acoustic role of the output duct in the discharge of a high pressure flow through diaphagms and perforated plates, in: 24th AIAA/CEAS Aeroacoustics Conference, 2018. Atlanta, GA, USA.
[10] C. Tam, M. Golebiowski, J. Seiner, On the two components of turbulent mixing noise from supersonic jets, in: 2nd AIAA/CEAS Aeroacoustics Conference, State Collage, PA, USA, 1996.
[11] J. Atvars, C. Wright, C. Simcox, Supersonic jet noise suppression with multitube nozzle/ejectors, in: 2nd AIAA Aeroacoustics Conference, Hampton, VA, USA, 1975.
[12] J. Atvars, G. Paynter, D. Walker, C. Wintermeyer, Development of acoustically lined ejector technology for multitube jet noise suppressor nozzles by model and engine tests over a wide range of jet pressure ratios and temperatures, NASA Contractor Report NASA CR 2382 (1974) 1–338.
[13] D. Regan, W. Meecham, Multitube turbojet noise-suppression studies using crosscorrelation techniques, J. Acoust. Soc. Am. 63 (6) (1978) 1753–1767.
[14] W. Meecham, D. Regan, Cross-correlation of noise produced inside a hot turbojet exhaust with and without suppression, in: 2nd AIAA Aeroacoustics Conference, 1975. Hampton, VA, USA.
[15] M. Harper-Bourne, M. Fisher, The noise from shock waves in supersonic jets, AGARD CP 131 (1973) 1–14.
[16] C. Tam, H. Tanna, Shock associated noise of supersonic jets from convergent-divergent nozzles, J. Sound Vib. 81 (3) (1982) 337–358.
[17] C. Tam, J. Seiner, J. Yu, Proposed relationship between broadband shock associated noise and screech tones, J. Sound Vib. 110 (2) (1986) 309–321.
[18] C. Bogey, C. Bailly, An analysis of the correlations between the turbulent flow and the sound pressure fields of subsonic jets, J. Fluid Mech. 583 (2007) 71–97.
[19] C. Tam, K. Viswanathan, K. Ahuja, J. Panda, The sources of jet noise: experimental evidence, J. Fluid Mech. 615 (2008) 253–292.
[20] S. Rienstra, A. Hirshberg, Fundamentals of Duct Acoustics, Technische Universiteit Eindhoven, Eindhoven, Netherlands, 2015.
[21] Y. Druon, Étude de la propagation guidée et du rayonnment acoustiques par les conduits d'éjection de turboréacteur (Study of the acoustic propagation and radiation from turbomachinery exhaust ducts analytical and numerical modelling), Ph.D. thesis, École Centrale de Lyon, 2006.
[22] A. Michalke, On the propagation of sound generated in a pipe of circular cross-section with uniform mean flow, J. Sound Vib. 134 (2) (1989) 203–234.
[23] A. Michalke, On experimental sound power determination in a circular pipe with uniform mean flow, J. Sound Vib. 142 (2) (1990) 311–341.
[24] U. Ingard, V. Singhal, Effect of flow on the acoustic resonances of an open-ended duct, J. Acoust. Soc. Am. 58 (4) (1975) 788–793.
[25] H. Levine, J. Schwinger, On the radiation of sound from an unflanged circular pipe, Phys. Rev. 73 (4) (1948) 383–406.

[26] Y. Ando, On the sound radiation from semi-infinite circular pipe of certain wall thickness, J. Sound Vib. 22 (1969) 219–225.
[27] M. Peters, A. Hirschberg, A. Reijnen, A. Wijnands, Damping and reflection coefficient measurements for an open pipe at low mach and low helmholtz numbers, J. Fluid Mech. 256 (1993) 499–534.
[28] G. Hofmans, R. Boot, P. Durrieu, Y. Aurégan, A. Hirschberg, Aeroacoustic response of a slit-shaped diaphragm in a pipe at low Helmholtz number, 1: quasi-steady results, J. Sound Vib. 244 (1) (2001) 35–56.
[29] P. Durrieu, G. Hofmans, G. Ajello, R. Boot, Y. Aurégan, A. Hirschberg, M. Peters, Quasisteady aero-acoutic response of orifices, J. Acoust. Soc. Am. 110 (4) (2001) 1859–1871.
[30] J. Kayser, R. Shambaugh, Discharge coefficients for compressible flow through small-diameter orificies and convergent nozzles, Chem. Eng. Sci. 46 (7) (1991) 1697–1711.
[31] V. Phong, D. Papamoschou, Acoustic transmission loss of perforated plates, in: 18th AIAA/CEAS Aeroacoustics Conference, Colorado Springs, CO, USA, 2012.
[32] K. Chen, Study on the acoustic transmission loss of a rigid perforated screen, Appl. Acoust. 47 (4) (1996) 303–318.
[33] T. Melling, The acoustic impedance of perforates at medium and high sound pressure levels, J. Sound Vib. 29 (1) (1973) 1–65.
[34] S. Stephens, S. Morris, A method for quantifying the acoustic transfer function of a ducted rotor, J. Sound Vib. 313 (2008) 97–112.
[35] Y. Pasco, S. Moreau, Sound radiation of a smoke-removal fan, in: Fan 2018, Darmstadt, April 2018. Germany.
[36] Z. Zhang, L. Mongeau, S. Frankel, Broadband sound generation by confined turbulent jets, J. Acoust. Soc. Am. 112 (2) (2002) 677–689.
[37] H. Tanna, An experimenatl study of jet mixing noise part 1: turbulence mixing noise, J. Sound Vib. 50 (3) (1977) 405–428.
[38] C. Bogey, S. Barré, V. Fleury, C. Bailly, D. Juvé, Experimental study of the spectral properties of near-field and far-field jet noise, Int. J. Aeroacoustics 6 (2) (2007) 73–92.
[39] A. Lafitte, Prédiction de l'aéroacoustique de jets subsoniques confinés à l'aide d'une méthode stochastique de génération de la turbulence (Prediction of confined jet noise relying on a stochastic turbulence generation method), Ph.D. thesis, École Centrale de Lyon, 2012.
[40] C. Bailly, C. Bogey, O. Marsden, T. Castelain, Subsonic and supersonic jet mixing noise, VKI Lecture Series 2016–04 (2016) 1–62.
[41] J. Panda, R. Seasholtz, Experimental investigation of density fluctuations in high-speed jets and correlation with generated noise, J. Fluid Mech. 550 (2002) 91–130.
[42] P. Nelson, C. Morfey, Aerodynamic sound production in low speed flow ducts, J. Sound Vib. 79 (2) (1981) 263–289.
[43] M. Verge, A. Hirchberg, R. Caussé, Sound production in recordlike instruments. II. A simulation model, J. Acoust. Soc. Am. 101 (5) (1997) 2925–2939.
[44] T. Emmert, P. Lafon, C. Bailly, Numerical study of self-induced transonic flow oscillations behind a sudden duct enlargement, Phys. Fluids 21 (2009) 1–15.
[45] F. Van Herpe, D. Crighton, P. Lafon, Noise generation by turbulent flow in a duct obstructed by a diaphragm, in: 1st AIAA/CEAS Aeroacoustics Conference, 1995. Munich, Germany.
[46] X. Gloerfelt, P. Lafon, Direct computation of the noise induced by a turbulent flow through a diaphragm in a duct at low Mach number, Comput. Fluid 37 (2008) 388–401.